Catalysis Today 430 (2024) 114539

Contents lists available at ScienceDirect

Catalysis Today

journal homepage: www.elsevier.com/locate/cattod

Towards sustainable environmental remediation: Ceftriaxone adsorption by titania derived from red mud

Mohamed Hosny [*,1], Justin S.J. Hargreaves [2]

School of Chemistry, Joseph Black Building, University of Glasgow, Glasgow G12 8QQ, United Kingdom

ARTICLE INFO

Keywords:
Red mud
Titania
Adsorption
Impregnation

ABSTRACT

In a world grappling with numerous challenges, including resource depletion, water shortages, soil pollution, and an escalating energy demand, it becomes imperative to leverage waste materials that hold potential benefits for such applications. One such waste material is red mud, a primary by-product of the aluminium production industry derived through the Bayer process. This by-product engenders significant environmental issues, notably water and soil pollution, owing to its high alkalinity. In response to this, the current study outlines the utilization of a red mud sample for the extraction of valuable metal oxides, specifically titania (TiO_2). This extracted TiO_2 aims to facilitate the adsorption of Ceftriaxone, a commonly discharged antibiotic in water systems. This work undertakes a comparative analysis evaluating the efficacy of commercially available TiO_2 against that extracted from the red mud sample in removing Ceftriaxone from model and tap water samples. The impregnation effect using two transition metals; iron and copper was investigated in the present study, details of which will be delineated in the subsequent sections. Additionally, the catalytic and photocatalytic efficiencies of one of these composites are investigated in this study.

1. Introduction

The Industrial Revolution, which commenced in the second half of the eighteenth century and stands as a defining chapter in recent human history, is perceived as a double-edged sword. On one side, it laid the foundation for unprecedented advancements in civilization, fostering progress, prosperity, and a dramatic surge in population. Conversely, it has been associated with a myriad of global environmental issues, including climate change and pollution affecting air, soil, and water resources, not to mention the pressing concern of biodiversity loss. These adverse effects are largely viewed as the unavoidable consequences of such expansive technological and industrial development [1, 2].

One of the principal industrial processes fundamental to the fabrication of a wide range of products is the Bayer process. This method, developed by Austrian scientist Carl Josef Bayer in 1888, facilitates the production of aluminium from bauxite ore. This innovation empowered humanity to create a diverse range of items including utensils, refrigerators, packaging materials, computers, airplanes, vehicles, and even components for pharmaceuticals. However, this advancement comes with its own set of drawbacks. Chief among these is the substantial generation of red mud, a waste product that can equal or even exceed the amount of aluminium produced, reaching a surplus of 50 to 80% [3]. Numerous countries around the world engage in aluminium production, with China as the biggest producer by manufacturing approximately 74 million tons in 2021 [4] resulting in the release red mud, which is the main byproduct of the aluminium production process, into the environment. China is the biggest contributing country to the red mud waste release in the world by 88 million tons out of 160 million tons in 2016 followed by other countries including Australia, Brazil, and India [5].

In the Bayer process, a solution of caustic soda (sodium hydroxide) is used to digest the bauxite and dissolve aluminium silicate, so a highly alkaline waste material of red mud is released into the environment [6]. Red mud could be reaching and contaminating numerous ecosystems because of its very high pH level [7]. Options for red mud storage include both wet and dry methods, each presenting its own set of challenges. Issues such as air transport and leaching can lead to

* Corresponding author.
E-mail address: 2706243m@student.gla.ac.uk (M. Hosny).
[1] ORCID ID: 0000–0001-6824–5459
[2] ORCID ID: 0000–0003-1926–9299

https://doi.org/10.1016/j.cattod.2024.114539
Received 28 November 2023; Received in revised form 11 January 2024; Accepted 16 January 2024
Available online 19 January 2024

groundwater and soil contamination, disrupt crop growth and production, adversely affect the global economy, and pose significant health risks to individuals [8]. In response to some of these issues, vegetative cover can be planted in red mud disposal regions to lessen the amount of hazardous dusts formed by dry red mud [9]. Consequently, it is concluded that storage of red mud is neither an environmentally friendly nor a cost-effective option. Thus, it is imperative to explore alternative methods to leverage this material, a task meriting the focused attention of the scientific community, especially given the red mud's rich content of valuable rare earth metals and various metallic oxides, including aluminium oxide (Al_2O_3), calcium oxide (CaO), titanium oxide (TiO_2), and different forms of iron oxide [10]. Therefore, red mud can be employed in construction and building materials including cement, concrete, and as fillers for road construction [11]. Furthermore, red mud and its metal oxides can be applied in different catalytic processes such as hydrogenation of CO_2 [12]. Additionally, these metal oxides can be utilized as adsorbents, photocatalysts in wastewater treatment as well as other applications as an alternative to disposing this highly toxic material within the environment.

The circular economy refers to an economic model that aims to minimize waste generation and maximize the reuse, recycling, and regeneration of materials in a closed-loop system by improving the efficiency of production processes and using waste materials from certain industries as inputs or a feedstock for other industries. It is an alternative to the traditional linear economy, where products are manufactured, used, and then discarded as waste [13]. In the circular economy, the focus is on creating a sustainable and regenerative systems that reduce environmental impact and relive pressure on natural resources to make them available for future generations by promoting the long-term resource efficiency, which is definitely in accord with the concept of sustainable development as first defined in 1987 and further clarified in the United Nations Conference on Environment and Development (earth summit) in 1992. Additionally, the circular economy is in line with the United Nations' sustainable development goals that were set in 2015. Of particular relevance; goals number 6 (clean water and sanitation) by reducing the amount of wastes released into water bodies, number 12 (responsible consumption and production) by extending the lifetime of products and designing them to be used in other applications by the end of their lifetime, and number 17 (partnerships for the goals) through the integration between different corporations and industries to use each other's waste materials.

TiO_2 nanoparticles, which can be sourced from red mud, are of interest due to their unique photochemical and thermal properties, as well as low production cost and low toxicity. TiO_2 can be produced by different methods such as hydrothermal synthesis, and it can have a porous structure and a high surface area that results in achieving a high adsorption capacity. TiO_2 is a widely used semiconductor material with strong photocatalytic properties, but its efficiency is limited to ultraviolet (UV) light due to its large bandgap energy (3–3.2 eV). TiO_2 can be easily modified or functionalized with various nanomaterials and transition metals or by coupling with other semiconductors to enhance its photocatalytic degradation efficiency under visible light as reported by Pelaez et al. [14] and adsorption of antibiotics as recently investigated by Gan et al. [15] who recorded an adsorption capacity of 888.57 mg/g of ciprofloxacin using TiO_2 modified with 10 wt% of copper ions. Another study was carried out by Sanguanpak et al. [16] to remove six different antibiotics including amoxicillin and others from hospital wastewater applying a composite of TiO_2 and a geopolymer of metakaolin, where the removal efficiency ranged between 38% and 75% by adsorption and up to 74 – 86% through the combination of adsorption and photodegradation.

Antibiotics represent a certain category of pharmaceuticals that are made specifically to be highly stable and to have a controlled biological impact at trace concentrations, rendering them highly toxic and persistent pollutants [17–19]. Consequently, the discharge of these pollutants into water bodies has exacerbated water pollution issues over

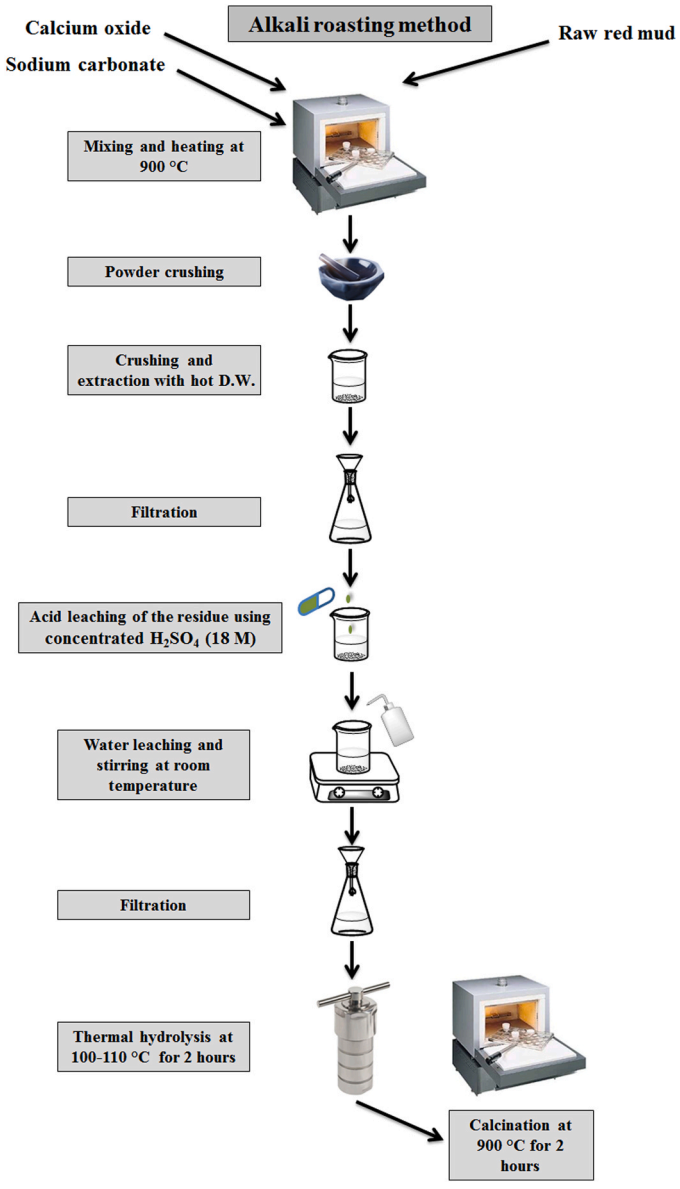

Scheme 1. Schematic illustration of TiO_2 synthesis by the alkali roasting method.

the last few decades [20,21]. In this regard, Ceftriaxone (CEF), a third-generation cephalosporin antibiotic, has proven effective in treating a variety of infections caused by gram-positive and gram-negative bacteria but unfortunately contributes to water pollution [22]. Therefore, the primary objective of this study is to explore the removal of CEF using TiO_2 nanoparticles, offering a comparative analysis between commercial TiO_2 and that derived from the red mud sample. By pursuing this avenue of research, we aim to adhere to the principles of sustainable synthesis and the circular economy, employing waste material like red mud to mitigate the impact of organic pollutants.

2. Materials and methods

2.1. Chemicals and reagents

Ferric nitrate nonahydrate ($Fe(NO_3)_3(H_2O)_9$) was purchased from Thermo Fisher scientific. Cobalt nitrate hexahydrate ($Co(NO_3)_2(H_2O)_6$), calcium oxide (CaO), sodium carbonate (Na_2CO_3), sulfuric acid (H_2SO_4), nitric acid (HNO_3), and sodium hydroxide (NaOH) were purchased from

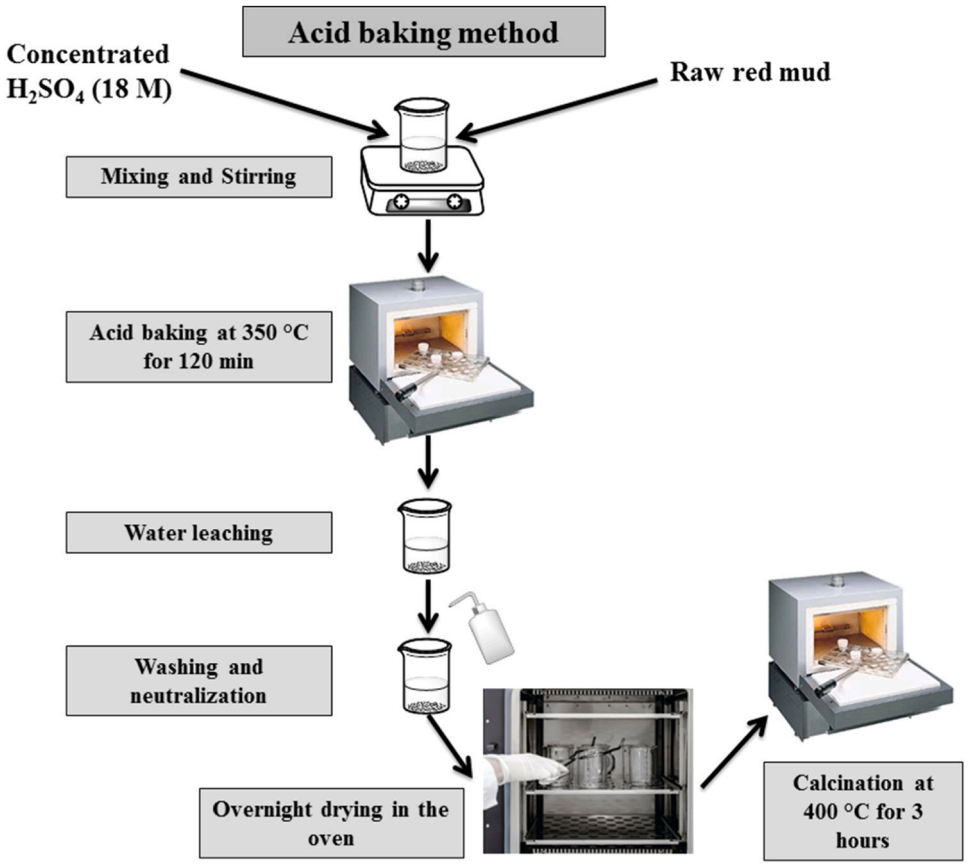

Scheme 2. Schematic illustration of TiO_2 synthesis by the acid baking method.

Fisher Scientific. Nickel nitrate hexahydrate ($Ni(NO_3)_2(H_2O)_6$) was purchased from Janssen Chimica. Copper nitrate trihydrate ($Cu(NO_3)_2(H_2O)_3$) from Riedel-de Haen (Honeywell). Zinc nitrate hexahydrate ($Zn(NO_3)_2(H_2O)_6$) from Alfa Aesar. Hydrogen peroxide (H_2O_2) 35% was purchased from Merck. Sodium nitrate ($NaNO_3$) was procured from Hopkin & Williams. Hydrochloric acid (HCl) was purchased from Honeywell Fluka. Commercial titania (Aeroxide P 25) was purchased from Thermo Fisher Scientific. Ceftriaxone sodium ($C_{18}H_{16}N_8Na_2O_7S_3$) antibiotic powder was purchased from Sandoz Pharmaceutical Company. A red mud sample from China (Shandong) was used as a source of TiO_2.

2.2. Extraction of TiO_2 from red mud

Two methods were used to extract TiO_2 from red mud; the first is called alkali roasting [23] as it starts with alkali addition, followed by acid leaching, water leaching, thermal hydrolysis, and calcination as shown in Scheme 1. Firstly, 5 g of red mud powder was mixed with 5 g of burnt lime (calcium oxide) and 5 g of soda ash (sodium carbonate) and then heated at 900 °C to dissolve the metal components contained within the sample. Subsequently, the produced powder was crushed, extracted with hot water, and filtered to remove the metal components. The residue was acid-leached using concentrated H_2SO_4 (18 M) in a ratio of 1 mL of acid to each gram of the produced residue. After digestion, the product was water-leached and stirred for one hour at room temperature with a solid-to-liquid ratio of 1:10 (w/v) followed by filtration. The filtrate was then subjected to thermal hydrolysis at 100–110 ℃ for 2 h to precipitate titanium hydroxide. Finally, the precipitate was filtered and calcined at 900 °C for 2 h to produce titanium oxide (TiO_2).

The second method was acid baking [24] in which 10 g of the red mud sample was mixed with 10 mL of concentrated H_2SO_4 (18 M) in a ratio of 1 mL of acid to each gram of red mud and stirred for 30 min to concentrate TiO_2 as shown in Scheme 2. Subsequently, the sample was transferred to a 50 mL crucible and the crucible was placed inside a muffle furnace for 120 min at 350 °C. After that, the baked product was left to leach in deionized water for 2 h with a liquid-to-solid ratio of 10 mL to 1 g to remove Fe, Al, and Si components and enrich TiO_2 in the sample. Afterward, water was decanted and the precipitated solid was washed several times with deionized water to neutralize its pH. Lastly, the washed precipitate was overnight-dried in the oven at 90 °C followed by calcination at 400 °C for 2 h to produce titanium oxide (TiO_2). TiO_2 produced either by the first or the second extraction method was modified with 2%, 5%, and 10 wt% Cu and Fe ions. 0.0076 g, 0.0190 g, and 0.0380 g of copper nitrate were mixed with 0.1 g of TiO_2 to prepare 2%, 5%, and 10% loadings, respectively. 0.0144 g, 0.0361 g, and 0.0723 g of iron nitrate were mixed with the same amount of TiO_2 to prepare 2%, 5%, and 10% loadings, respectively. Finally, these composites were dried.

2.3. Characterization techniques

The crystalline phase composition of the synthesized materials was investigated by a Miniflex powder diffractometer (Rigaku) benchtop X-ray diffractometer (XRD) in a range of 5–85° 2θ with a step size of 0.01500 and a counting rate of 20°/min. Surface area was determined from physisorption isotherms applying the BET method using a Quadrasorb Automated Surface Area & Pore Size Analyzer (Evo) applying nitrogen gas as an adsorbate at – 196 °C, degassing temperature (130 °C), time (16 h), and 1 °C per minute ramp rate. Inductively coupled plasma (ICP) analysis was carried out using a MY2131CP01 Agilent Technologies instrument to determine the concentration of leached metal ions including copper at 327 nm and iron at 238 nm. The ICP measurements were repeated three times and the average metal concentrations were detected. The main functional groups of CEF and

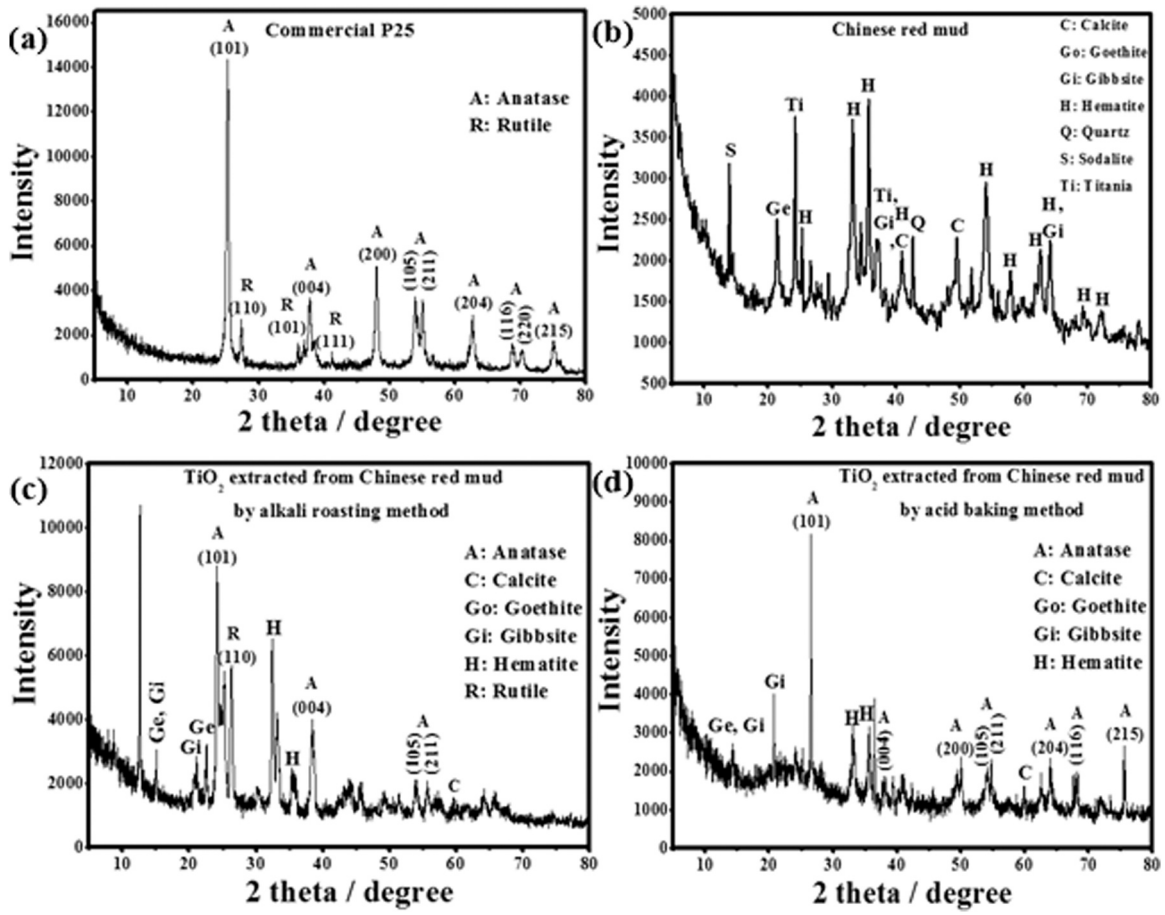

Fig. 1. XRD pattern of P25 **(a)** XRD patterns of Chinese red mud **(b)**, TiO_2 extracted from Chinese red mud by the alkali roasting method **(c)**, and TiO_2 extracted from Chinese red mud by the acid baking method **(d)**.

TiO_2-based composite were examined by Fourier Transform Infrared Spectroscopy (FTIR-8400S Shimadzu).

2.4. Adsorption of CEF using titania and its composites

For the adsorption experiments, the first and the most important parameter was the pH which was adjusted by 0.01 M HCl and 0.01 M NaOH using a pH meter (Thermo Scientific), so a wide range of pH levels including 3, 5, 7, 9, and 11 was used to test the adsorption efficiency using 20 mL of CEF with a concentration of 25 ppm in dark conditions. In addition, other factors were tested including the initial concentration of CEF (15, 25, 50, 75, and 100 ppm), the adsorbent dose (0.005, 0.0075. and 0.01 g), and the stirring rate (0 up to 1200 rpm) for the sake of removal optimization.

The percentage of CEF adsorption was calculated by the following formula:

$$\% \text{ Adsorption} = 100 \times (A_0 - A)/A_0 \quad (1)$$

where A_0 refers to the initial CEF concentration that was measured by a UV–Vis spectroscopy (UV-1800 Shimadzu) over a scan range of 200 – 800 nm, while A refers to the CEF concentration after a certain time that measured by the same instrument but after separating the adsorbent by centrifugation (TD4A-WS Desk centrifuge).

The adsorption capacity is calculated by the following equation:

$$\text{Adsorption capacity (mg/g)} = [\text{Co - Ce}) /\text{m}] \text{ x V} \quad (2)$$

where Co is the initial concentration of CEF in ppm (mg/L), Ce is the concentration at equilibrium in ppm (mg/L), m is the mass of the adsorbent in grams (g), and V is the volume of solution in liters (L).

2.5. The catalytic degradation of CEF through Fenton degradation, photocatalysis, and photo-Fenton degradation by 5% Fe 5% Cu-TiO_2

In the Fenton degradation experiments, the pH of five CEF solutions with a volume of 20 mL and a concentration of 25 ppm was varied over a range of 3 – 11. Subsequently, 0.01 g of 5% Fe 5% Cu-TiO_2 was added to each solution and then the solutions were subjected to stirring for 30 min at 800 rpm in dark conditions for the adsorption-desorption equilibrium. The used experimental conditions are the optimum conditions as discussed in Section 3.4. Then 1 mL of H_2O_2 (0.1 M) was added to each solution and stirred for 120 min. The adsorption efficiency after 30 min of dark adsorption and the catalytic degradation efficiency after each 30 min of H_2O_2 addition for 120 min were measured using the above-mentioned UV-Vis spectroscopy and Eq. 1. Also, blank experiments were conducted using H_2O_2 without adding 5% Fe 5% Cu-TiO_2 over the same pH range (3−11) to test its catalytic degradation efficiency.

Regarding the photocatalytic degradation of CEF, the experiments were only conducted for 120 min after 30 min of adsorption in dark conditions at pH 3, which is the optimum pH as further discussed in Section 3.4, along with the other optimum reaction conditions using 5% Fe 5% Cu-TiO_2 under the illumination of an LED lamp (λ = 400–700 nm, 60 Watt) as the source of visible light with a distance of 10 cm between the lamp and the surface of the CEF solution. Moreover, the photo-Fenton catalytic degradation efficiency of 5% Fe 5% Cu-TiO_2 was tested using H_2O_2 and visible light at pH 3. In addition, two blank experiments were run without adding 5% Fe 5% Cu-TiO_2; one of them just by H_2O_2 and the other by H_2O_2 with visible light. All absorbance measurements were performed using UV-Vis spectroscopy.

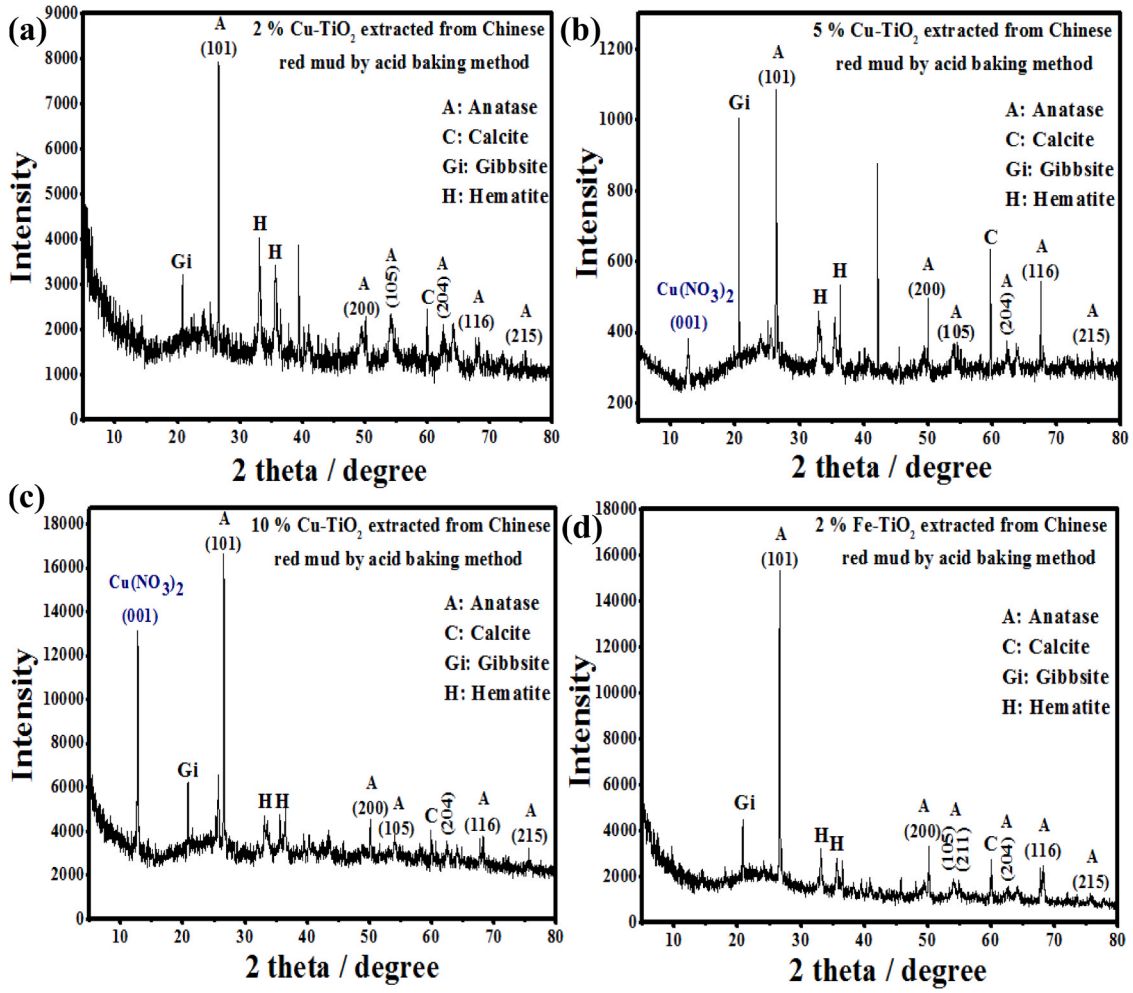

Fig. 2. XRD patterns of 2% Cu-TiO_2 (a), 5% Cu-TiO_2 (b), 10% Cu-TiO_2 (c), 2% Fe-TiO_2 (d), 5% Fe-TiO_2 (e) 10% Fe-TiO_2 (f), and 5% Fe 5% Cu-TiO_2 (g) extracted from Chinese red mud by the acid baking method.

2.6. Determination of point of zero charge (PZC) of titania and other adsorbents by salt addition method

A simple procedure, the salt addition method [25], was undertaken to determine the PZC of TiO_2 and its complexes at which the net surface charge is zero, and hence the surface charge is positive at pH levels below the PZC and negative at pH levels higher than the PZC. The PZC was determined by mixing these materials with sodium nitrate with a low concentration (0.1 M) over a pH range from 2 to 12 for 24 h using a magnetic stirrer. The pH level was adjusted using 0.1 M HNO_3 and 0.01 M NaOH. Subsequently, the pH of each suspension was measured after filtering the adsorbents. The difference between the initial and final pH values was plotted on the ordinate axis with the initial pH level plotted on the abcissa axis to determine the PZC.

3. Results and discussion

3.1. XRD analysis

The XRD pattern of commercial TiO_2 (P25) exhibited the presence of both anatase and rutile phases as shown in Fig. 1.**a**. Most of the peaks apparent related to the anatase phase, whereas some peaks at 27.30°, 36.00°, and 41.10° representing the reflections of (110), (101), (111) were attributed to the rutile phase in accordance with [26] [JCPDS file number 21–1272].

The XRD pattern of the raw Chinese red mud indicated the presence of some mineral phases including sodalite at 13.91°, calcite at 41.00°and 49.65°, goethite at 21.45°, gibbsite at 37.26° and 64.16°, hematite at 25.35°, 33.20°, 35.72°, 41.00°, 54.12°, 58.02°, 62.54, 64.16, and 69.39°, 72.11°, quartz at 42.63°, and most importantly titania at 24.24° and 37.26° (Fig. 1.**b**). Such a composition was in agreement with Gu et al. [27] who characterized the same red mud sample from the same area (Shandong) in China. Upon conducting the same analysis for the extracted titania from Chinese red mud using the alkali roasting method, it was clear that titania was impure as there were some mineral phases still present as shown in Fig. 1.**c**, and the titania phase was mostly anatase. However, a characteristic peak corresponding to rutile was observed at 26.34° along with other unknown peaks. In contrast to the XRD pattern of the TiO_2 extracted by the alkali roasting method, TiO_2 extracted by the acid baking method exhibited a purer crystalline phase composition and it was only present in the form of anatase (Fig. 1.**d**).

The appearance of a rutile phase in TiO_2 extracted by the alkali roasting method is attributed to the very high temperature used in this method that reached 900 °C compared to the lower temperature used in the acid baking method that was 400 °C. Such a high temperature results in conversion of anatase into rutile. Moreover, the purer crystalline phase composition of TiO_2 produced by acid baking method is related to its simpler and fewer steps compared to the alkali roasting method. These fewer steps constitute a lower likelihood of introducing additional contaminants or impurities during the extraction process.

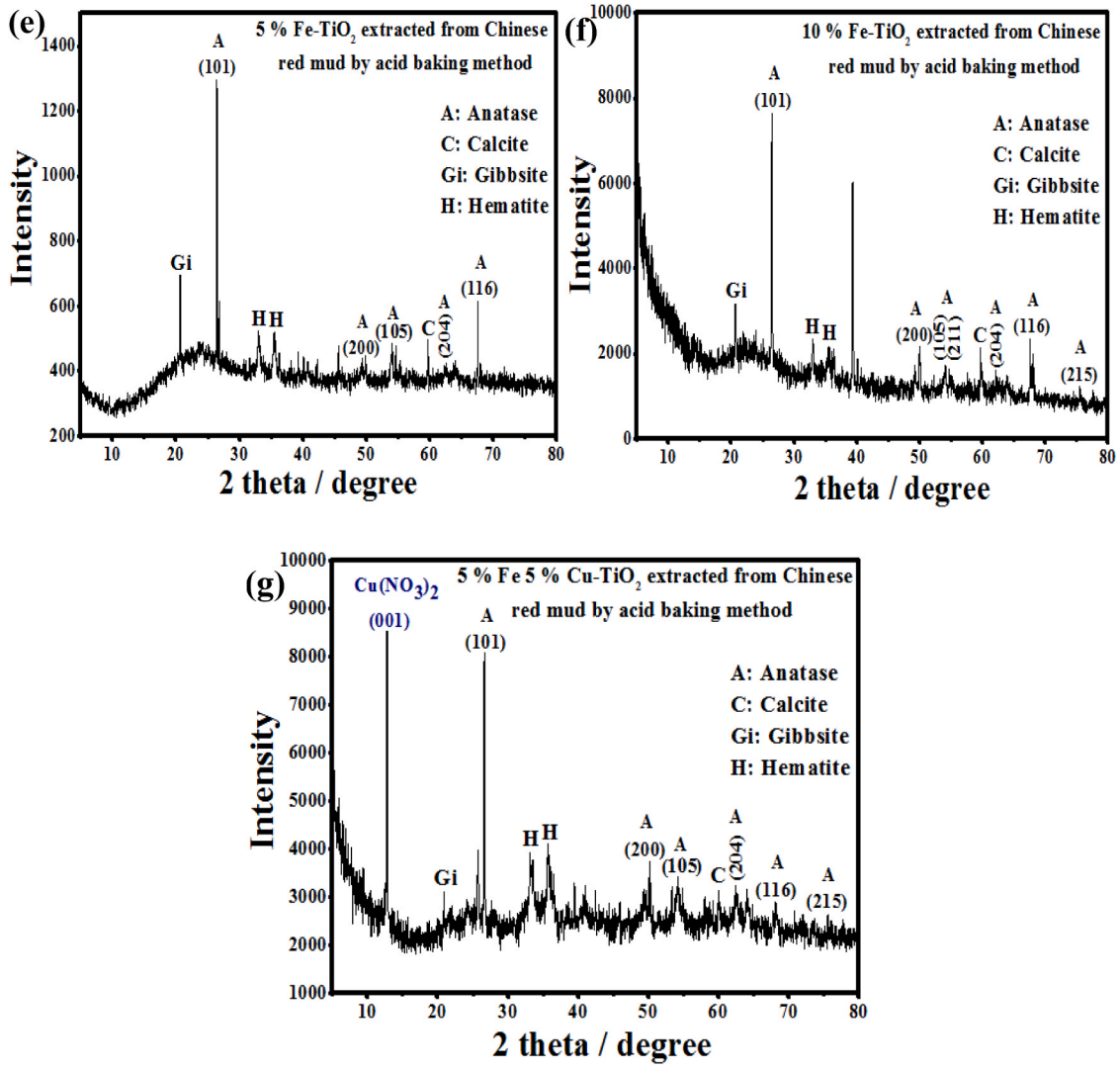

Fig. 2. (*continued*).

XRD patterns of Cu-TiO_2 samples with three different impregnation ratios (2%, 5%, and 10%) using TiO_2 extracted by acid baking method, showed a slight difference when the higher impregnation percentages of copper (5% and 10%) were used (Fig. 2.**a-c**) compared to the pristine TiO_2 as some distinguishing peaks such as that of (001) at 12.70°, which is the major XRD reflection of hydrated copper nitrate salts [28], was observed in these two composites. The intensity of the copper nitrate peak was higher when the higher copper percentage (10%) was used (Fig. 2.**c**). The same peak was also observed in 5% Fe 5% Cu-TiO_2 as shown in Fig. 2.**g** when 5% of copper nitrate was used to impregnate TiO_2 simultaneously with 5% of iron nitrate. It has to be mentioned that the appearance of copper nitrate peaks is attributed to the observed adsorption efficiencies of the TiO_2 composites containing the high percentages of this salt at alkaline pH levels as will be further discussed and indicated in Fig. 5 which shows the efficiencies of TiO_2 composites and Fig. 6 that presents the performance of the metal salt precursors. No major changes were observed in the structure of Fe-TiO_2 composites as shown in Fig. 2.**(d-f)**. In addition, it could be suggested that the intensity and the position of TiO_2 peaks did not change after the impregnation process with any of the abovementioned metals as the technique used for impregnation was a wet deposition reaction in which the metal salt precursors are mixed with the already synthesized TiO_2, not during the synthesis process.

3.2. BET analysis

BET analysis indicated that the surface area of the commercial TiO_2 (P25) was 56 m^2/g (Fig. 3.a) compared to 139 m^2/g for the TiO_2 extracted from Chinese RM by the acid baking method as shown in Fig. 3.b. Consequently, the adsorption efficiency of the extracted TiO_2 was expected to be generally higher than P25. It should be noted that impregnation of TiO_2 with transition metals might increase or decrease its surface area based on several factors including the concentration of the impregnated metal, synthesis or impregnation procedures, and specific characteristics of both of impregnating metal and TiO_2. 10% Fe-TiO_2 and 10% Cu-TiO_2 exhibited surface areas of 93 m^2/g (Fig. 3.c) and 92 m^2/g (Fig. 3.d), which are lower than that of TiO_2 extracted from Chinese red mud (139 m^2/g) by the acid baking method. Similarly, the surface areas of 2% Cu-TiO_2, 2% Fe-TiO_2, 5% Cu-TiO_2, and 5% Fe-TiO_2 were lower than the pristine TiO_2 as they were 53 m^2/g, 114 m^2/g, 58 m^2/g, and 65 m^2/g (figures are not shown). Concomitantly with the abovementioned results, the surface area of 5% Fe 5% Cu-TiO_2 dropped to 56 m^2/g (Fig. 3.e). The major trend of the diminished surface areas of all materials observed in the current study could be attributed to the occupation of TiO_2 surface sites by the impregnating metals along with the filling of TiO_2 pores with these metals resulting in the formation of less accessible surfaces, which is consistent with the observation of Di Paola et al. [29]. The obtained results are also in agreement with

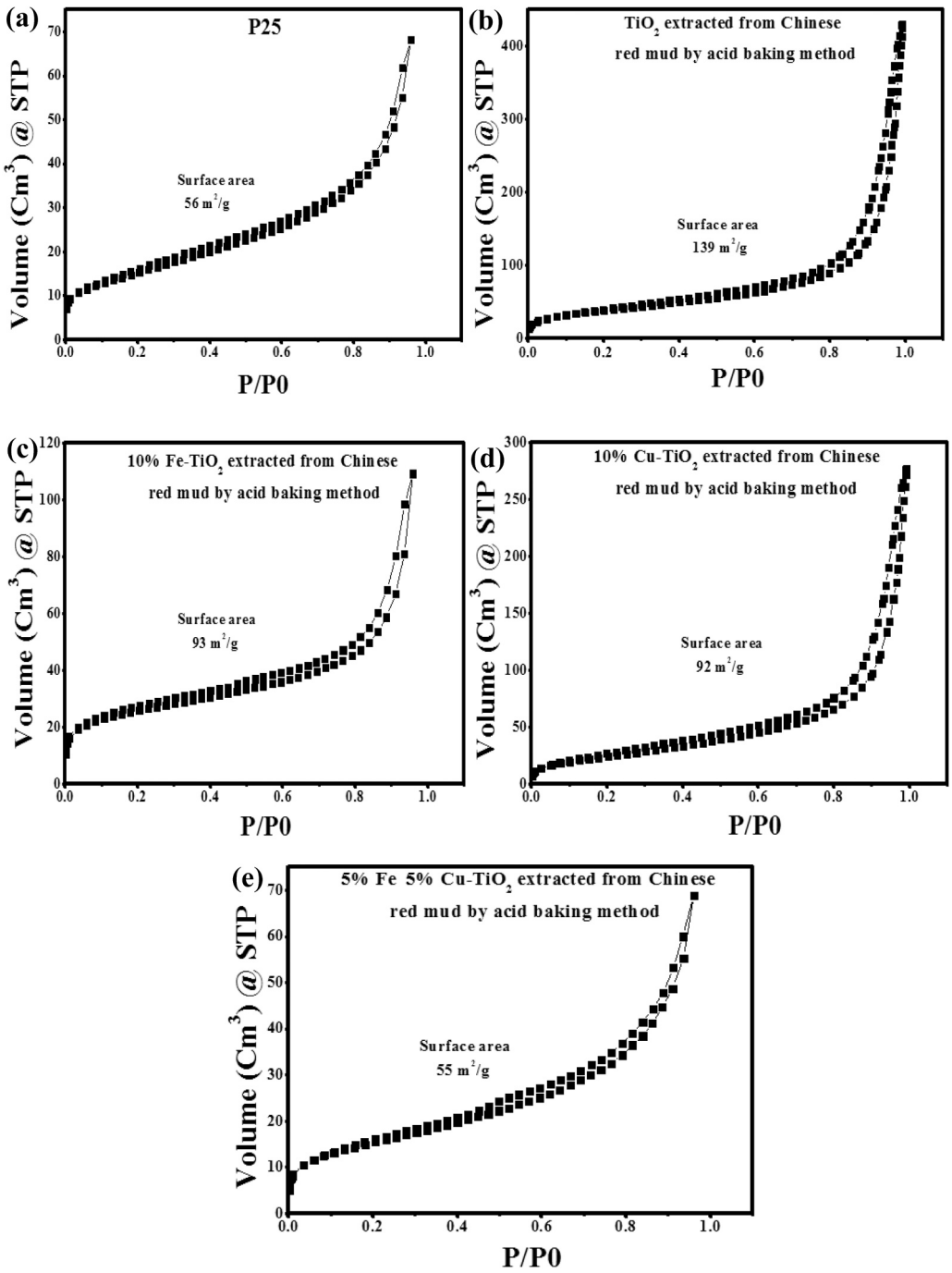

Fig. 3. Nitrogen physisorption isotherms of P25 (a), TiO_2 extracted from Chinese RM by the acid baking method (b), 10% Fe-TiO_2 (c), 10% Cu-TiO_2 (d), and 5% Fe 5% Cu-TiO_2 (e) extracted from Chinese red mud by the acid baking method.

Abdelouahab Reddam et al. [30] who observed decreased surface area of a commercial titania sample (P25) after being impregnated with copper, iron, and manganese. It has to be clarified that the surface area is only shown in Fig. 3 for the composites that showed promising results in CEF adsorption.

3.3. SEM and EDX analysis

SEM analysis revealed a needle-like morphology for TiO_2 extracted employing the alkali roasting method (Fig. 4.a) compared to the irregular morphology of TiO_2 extracted by the acid baking method (Fig. 4.c). EDX analysis was used to study the elemental composition of TiO_2 samples extracted by both methods to determine which sample is purer. As shown in Fig. 4.b, the elemental composition of TiO_2 extracted by the alkali roasting method included sodium and calcium, which were not detected in the EDX spectrum of TiO_2 extracted by the acid baking method (Fig. 4.d). The detection of both elements in Fig. 4.b could be attributed to the use of a large number of chemicals in the alkali roasting method. Therefore, the higher purity of TiO_2 extracted by the acid baking method was confirmed by detecting fewer elements in the EDX spectrum.

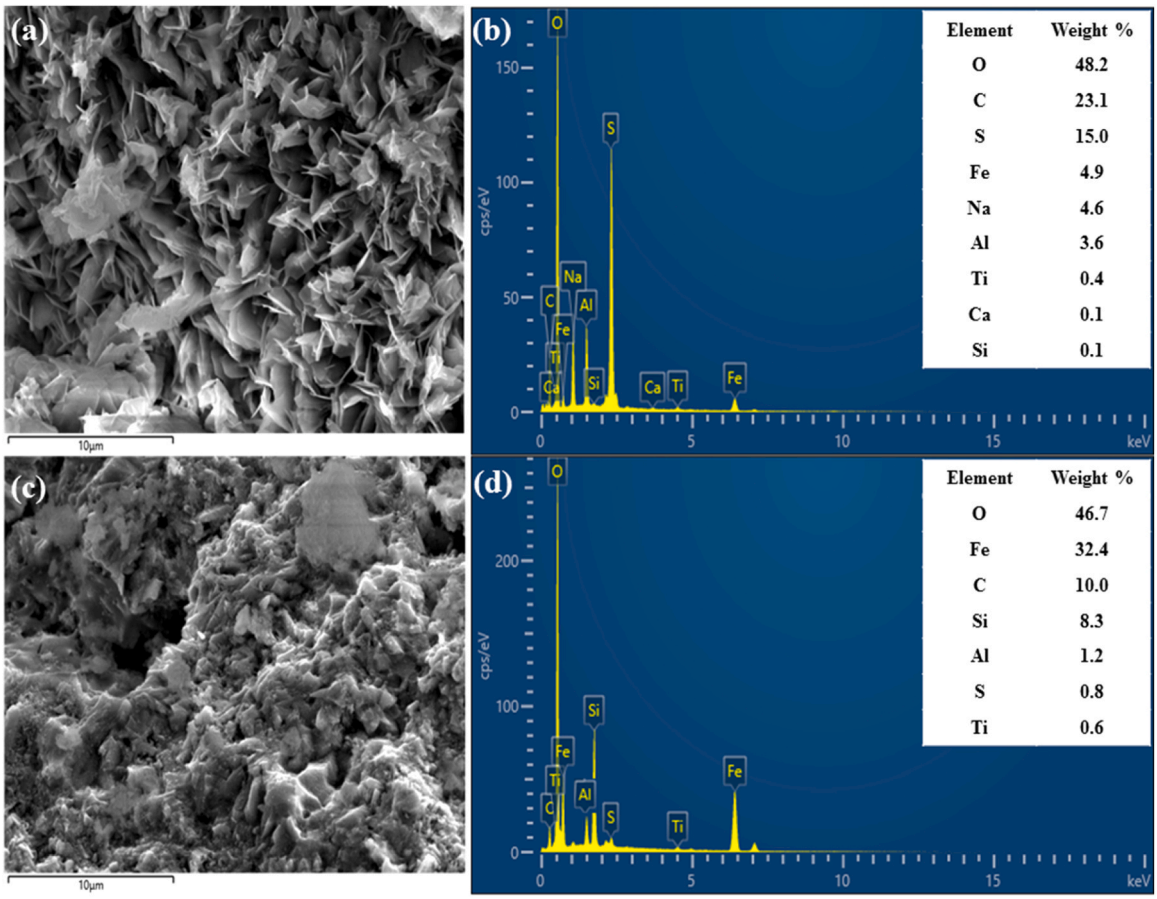

Fig. 4. SEM images and EDX spectra of TiO_2 extracted by alkali roasting method **(a** and **b)** and TiO_2 extracted by the acid baking method **(c** and **d)**.

3.4. Removal of CEF by TiO_2 and TiO_2 composites

3.4.1. A comparison between the efficiency of red mud-extracted TiO_2 and commercial TiO_2 in CEF adsorption

When a comparative study was conducted to determine the CEF adsorption efficiency by three samples of TiO_2, it was clear that TiO_2 extracted from Chinese RM by the acid baking method (Fig. 4.**b**) had a high efficiency over most of the pH levels, although P25 was slightly more efficient at pH 3 as shown in Fig. 5.**a**. Therefore, the Chinese RM based-TiO_2 was further investigated through impregnation with various transition metals including Fe^{3+}, Co^{2+}, Ni^{2+}, Cu^{2+} and Zn^{2+}. Such an impregnation was meant to enhance the adsorption efficiency whether by increasing the PZC (Table 1) or by causing complex formation. The selection of these metals was based on their availability. It has to be mentioned that the adsorption trend of TiO_2 extracted by the acid baking method (Fig. 5.**b**) was similar to that of P25 as the adsorption efficiency dropped with increasing pH. This behavior is further discussed in the next few paragraphs. In contrast, TiO_2 extracted by the alkali roasting method exhibited a completely opposite trend as the adsorption efficiency was improving by increasing the pH level (Fig. 5.**c**). Such a result could be accredited to the high impurity of TiO_2 as shown in the EDX spectrum in Fig. 4.**a**.

A wide survey was undertaken using an impregnation percentage of 10 wt% of each one of the above-mentioned transition metals. Three out of the five metals including Co^{2+}, Ni^{2+}, and Zn^{2+} did not show promising adsorption results and they had a negative impact on the efficiency of TiO_2 at acidic and neutral pH levels as shown in Fig. 6.a-c. Therefore, the three metals were excluded from further studies and the focus was only on the composites of Fe^{3+} and Cu^{2+} since the performance of 10% Fe-TiO_2 and 10% Cu-TiO_2 was better over most of the investigated pH levels as it will be shown in Fig. 7.

The adsorption results showed that the impregnation using copper ions with a percentage of 2%, 5% and 10% only improved the performance of TiO_2 extracted from Chinese red mud in neutral and alkaline media (Fig. 7.a, b and c). Among the three percentages, 10% Cu-TiO_2 showed the best performance, which can be attributed to the enhanced electrostatic attraction towards the negatively charged CEF molecules as a result of the high PZC value of 6.3 compared to 5.9 and 3.7 for 5% Cu-TiO_2 and 2% Cu-TiO_2, respectively. While using iron with a loading percentage of 2% did not improve the adsorption efficiency at any pH level as shown in Fig. 7.d, which could be related to the increased electrostatic repulsion indicated by its low PZC value that is 3.3. Regarding 5% Fe-TiO_2, the performance was generally better than that of 2% Fe-TiO_2 possibly due to the improved electrostatic attraction that was even extended to pH 11 by showing 10% of CEF adsorption (Fig. 7.e) indicated by the slightly higher PZC value (3.7). Similarly to 10% Cu-TiO_2, the performance of 10% Fe-TiO_2 was better than the other loading percentages of iron as it increased the adsorption efficiency of TiO_2 over the whole pH range except at pH 11 (Fig. 7.f) because of its higher PZC value (4.2) resulting in a further improved electrostatic attraction. The pH of pure CEF solution is 5.8.

According to the above-mentioned results, it was unequivocal that the electrostatic attraction between the positively charged TiO_2 complexes and the negatively charged CEF molecules is improved by increasing the metal loading. In addition, it was clear that the adsorption efficiency of Cu-TiO_2 complexes was better at the alkaline pH levels as could be accredited to their higher PZC values, whereas Fe-TiO_2 complexes are better over the acidic pH range with lower PZC values that could be accredited to the higher positive charge of Fe^{3+} compared Cu^{2+} resulting in better electrostatic attraction at low pH levels. Therefore, a new composite made of both Cu and Fe was synthesized by using both metals with a metal loading of 5% to produce 5% Fe 5% Cu-TiO_2 to

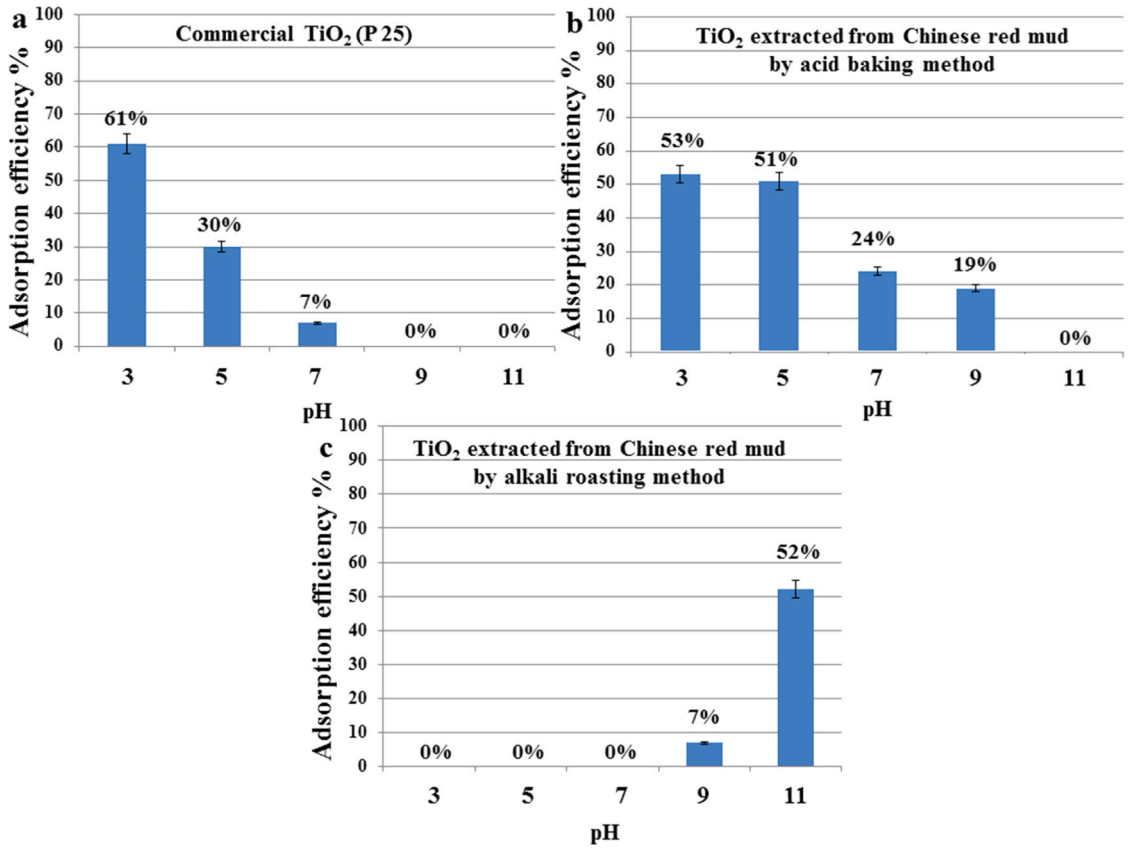

Fig. 5. A comparison between the adsorption efficiency of P25 **(a)**, TiO_2 extracted by the acid baking method from Chinese RM **(b)**, and TiO_2 extracted by the alkali roasting method from Chinese red mud **(c)** after 30 min. [C_o = 25 ppm, stirring rate = 800 rpm, T = 25 °C, and dose = 0.01 g].

Table 1
The point of zero charge (PZC) of the adsorbents used in the current study.

Adsorbent	Point of zero charge (PZC)
P25	4.9
TiO_2 extracted from Chinese RM by the acid baking method	4.0
10% Cu-TiO_2	6.3
10% Fe-TiO_2	4.2
5% Cu-TiO_2	5.9
5% Fe-TiO_2	3.7
2% Cu-TiO_2	3.7
2% Fe-TiO_2	3.3
5% Fe 5% Cu-TiO_2	5.8

improve the adsorption efficiency over the whole pH range. As shown in Fig. 7.g, 5% Fe 5% Cu-TiO_2 showed a better performance compared to all of the previously discussed materials as the adsorption efficiency was above 50% over most of the pH range, which could be accredited to the synergistic effect between copper and iron ions. Even though the surface area of this material was less than that of pristine TiO_2 (139 m^2/g) similar to 10% Fe-TiO_2 and 10% Cu-TiO_2 as it is 55 m^2/g, the PZC was found to be 5.8 indicating the possible improved electrostatic attraction. So based on these results, 5% Fe 5% Cu-TiO_2 was selected to be further investigated using more factors other than the variation in pH level. It has to be mentioned that the adsorption capacity of 5% Fe 5% Cu-TiO_2 was 29, 27.5, 27, 26, and 25 mg/g at pH levels 3, 5, 7, 9, and 11, respectively, as shown in Fig. 7.h.

According to Aleksić et al. [31] CEF has four acid dissociation constants (p*Ka*) values including pKa_1 2.37 of the carboxylic group, pKa_2 3.03 of the aminothiazole species, and pKa_3 4.21 of the hydroxytriazinone species, along with pKa_4 10.74 of the amide functional group. Therefore, CEF molecules are in a cationic form at very low pH levels, and by increasing the pH these molecules will be in a zwitterionic form, and by further increasing the pH they will be in an anionic form, which is in accord with Zaki and Hafez [32] who reported the negative charge of CEF molecules at pH 6. When 5% Fe 5% Cu-TiO_2 was tested at pH 1 and pH 2 (figures are not shown) to clarify the speciation of CEF at different pH levels, the adsorption efficiency was found to be 5% and 30%, respectively. This result indicated the electrostatic repulsion between the adsorbent and the positively charged CEF molecules at very low pH levels such as 1, which is less than the lowest p*Ka* of the carboxylic group of CEF (2.37). Therefore, it was suggested that the amino group of the aminothiazole side chain of CEF molecules is protonated by gaining protons (H^+) in a highly acidic medium becoming positively charged. Then by increasing the pH to 2, the de-protonation started to occur, the carboxyl group lost a proton and became negatively charged, and CEF molecules showed the zwitter ionic form, which resulted in an enhanced electrostatic attraction between CEF molecules and 5% Fe 5% Cu-TiO_2 indicated by the improved adsorption efficiency from 5% to 30%. A further increase in the pH level to 3 and even higher led to the de-protonation of the amino and hydroxyl groups of CEF molecules by losing their protons and increasing the overall negative surface charge of CEF molecules, resulting in their electrostatic attraction toward all of the positively charged adsorbents such as 5% Fe 5% Cu-TiO_2. By increasing the pH of the CEF solution more than the PZC values of these adsorbents, they become negatively charged and result in an electrostatic repulsion with negatively charged CEF molecules and leading to a drop in the adsorption efficiency. The proposed structures of CEF at different pH levels are shown in Fig. 8.

Blank experiments were conducted using the salt precursors of copper and iron nitrates to investigate their efficiencies and also to determine if there is a synergistic effect between these precursors and TiO_2. Copper nitrate exhibited CEF removal over the whole pH range as shown

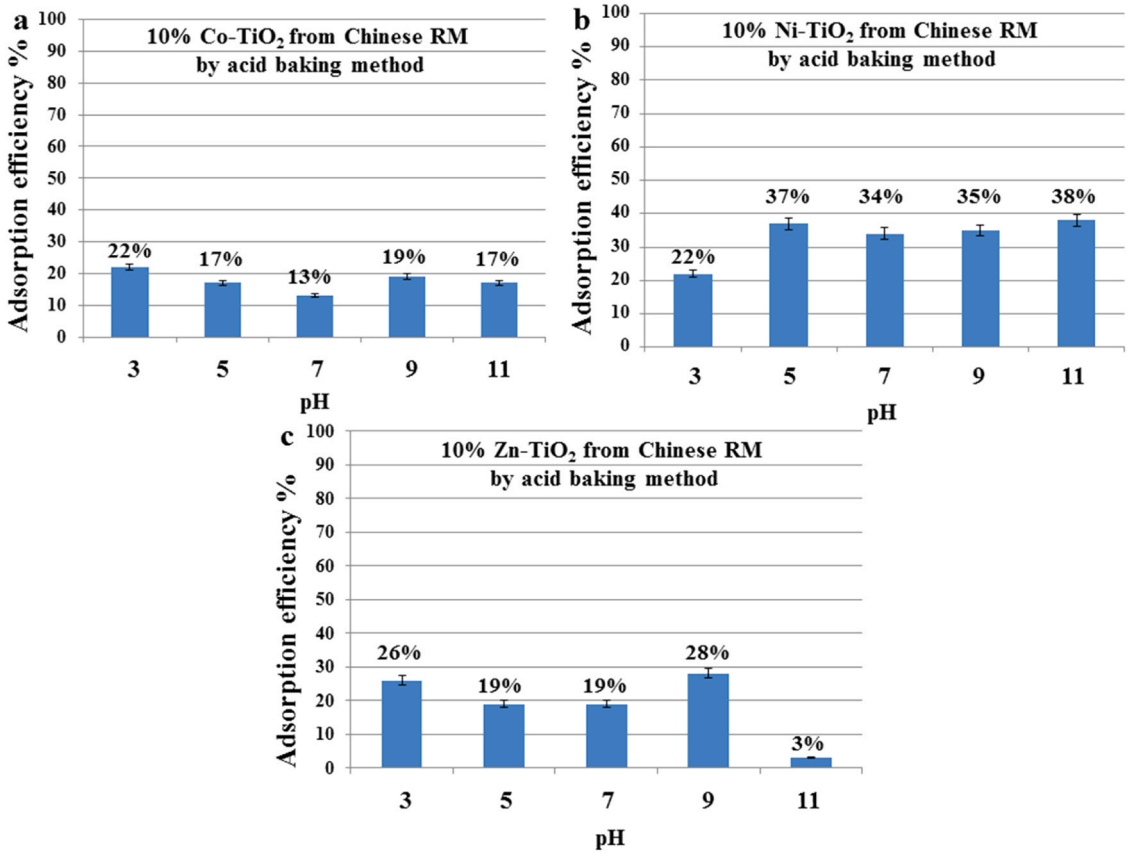

Fig. 6. CEF adsorption efficiency after 30 min by 10% Co-TiO_2 (a), 10% Ni-TiO_2 (b), and 10% Zn-TiO_2 (c) using TiO_2 extracted from Chinese RM by the acid baking method. [C = 25 ppm, stirring rate = 800 rpm, T = 25 °C, and dose = 0.01 g].

in Fig. 9.a. On the other hand, the iron precursor had no effect at all (Fig. 9.b). Such a result could be another reason behind the observed efficiency of Cu-TiO_2 complexes and 5% Fe 5% Cu-TiO_2 at alkaline pH levels compared to Fe-TiO_2 complexes. In other words, the residue of copper nitrate that remained in Cu-TiO_2 complexes and 5% Fe 5% Cu-TiO_2 as confirmed in the XRD patterns (Fig. 2.b, c and g) was responsible for the observed adsorption efficiencies at alkaline pH levels.

3.4.2. Catalytic and photocatalytic degradation of CEF using 5% Fe 5% Cu-TiO_2

The catalytic efficiency of 5% Fe 5% Cu-TiO_2 in the degradation of CEF using H_2O_2, which was used as an oxidant, in Fenton degradation, was investigated over the same pH range of adsorption experiments (3−11). The obtained results after 120 min of adding H_2O_2 indicated a slight increase in the removal efficiency of CEF over the whole pH range after running adsorption experiments for 30 min to establish the adsorption/desorption equilibrium, which were undertaken before adding H_2O_2. As shown in Fig. 10.a, the increase in the removal efficiency was just from 58% to 69% at pH 3, 55% to 69% at pH 5, 54% to 68% at pH 7, 52% to 58% at pH 9, and from 50% to 56% at pH 11. Such a result indicated the low catalytic efficiency of 5% Fe 5% Cu-TiO_2 in activating H_2O_2 and producing free radicals such as hydroxyl radicals (•OH) that could be resulting in high degradation efficiencies if produced in large numbers. A set of blank experiments was carried out over the same pH range using only H_2O_2 where the removal efficiencies were 10% or even less as displayed in Fig. 10.b indicating the need for a catalyst to activate H_2O_2.

Regarding the photocatalytic efficiency of 5% Fe 5% Cu-TiO_2, it was tested under the illumination of visible light for 120 min after 30 min of adsorption in dark conditions. This experiment was conducted only at pH 3 as it is the pH level at which the highest efficiency was recorded. As shown in Fig. 10.c, the efficiency just increased from 58% to 66% indicating the low photocatalytic activity of 5% Fe 5% Cu-TiO_2 in generating reactive oxygen species under visible light. Upon using visible light without the catalyst (Fig. 10.c), there was no degradation at all indicating the high persistency of CEF molecules under visible light. Subsequently, an experiment of photo-Fenton degradation was carried out to investigate the synergistic effect of H_2O_2 and visible light in degrading CEF molecules in the presence of 5% Fe 5% Cu-TiO_2 as catalyst. The degradation efficiency increased from 58% after 30 min of adsorption to 74% after 120 min after adding H_2O_2 and using visible light (Fig. 10.c), which is not a significant increase as it was expected. Lastly, a blank experiment using both H_2O_2 and visible light attained a degradation efficiency of 11% (Fig. 10.**c**) to further confirm the very unlikely degradation of CEF molecules when exposed to visible light. So based on all of these results, it was decided that it is better to use 5% Fe 5% Cu-TiO_2 only as an adsorbent.

3.4.3. Effect of time, initial concentration of CEF, adsorbent dose, and stirring rate on CEF adsorption using 5% Fe 5% Cu-TiO_2

The extent of CEF adsorption with time was investigated in the current study using 5% Fe 5% Cu-TiO_2. As shown in Fig. 11, the adsorption was fast as the adsorption efficiency was 17% after just one minute and then it reached the equilibrium just after 30 min by exhibiting 58% of CEF adsorption. Subsequently, the extent was almost the same even after 75 min. This behavior could be attributed to the availability of a high number of surface active sites at the start of the adsorption process. Afterward, CEF molecules were continuously adsorbed on these surface sites till reaching the equilibrium at which there are no further available surface sites to adsorb CEF molecules. Such a result indicated the acceptable efficacy of 5% Fe 5% Cu-TiO_2 as it did not take so much time to reach the equilibrium, which was only after

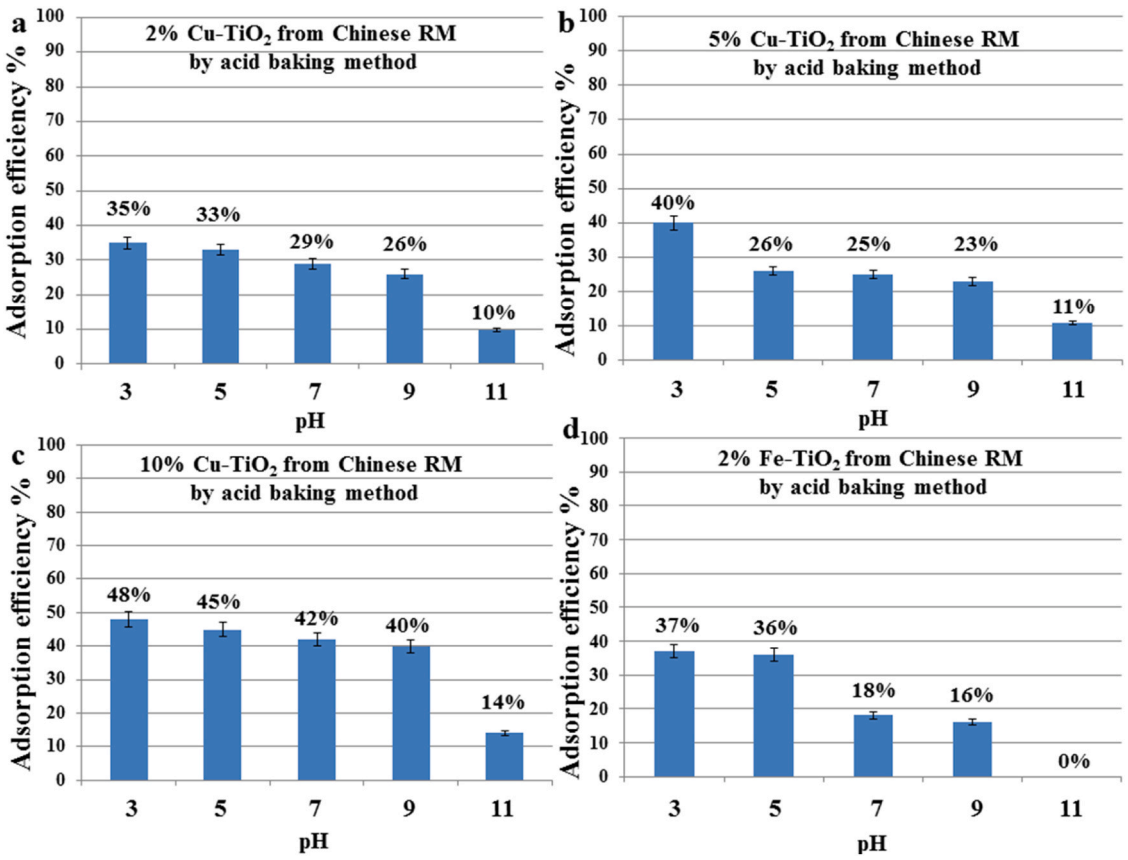

Fig. 7. CEF adsorption efficiency after 30 min by 2% Cu-TiO_2 (a), 5% Cu-TiO_2 (b), 10% Cu-TiO_2 (c), 2% Fe-TiO_2 (d), 5% Fe-TiO_2 (e), 10% Fe-TiO_2 (f), 5% Fe 5% Cu-TiO_2 (g), and CEF adsorption capacity by 5% Fe 5% Cu-TiO_2 (h) using TiO_2 extracted from Chinese RM by the acid baking method. [C_o = 25 ppm, stirring rate = 800 rpm, T = 25 °C, and dose = 0.01 g].

30 min. The adsorption capacity of this composite ranged from 8.5 mg/g to 29 mg/g by increasing the adsorption time from 1 min to 30 min, and then it remained constant up to 75 min as shown in Fig. 11.

The effect of other factors including the initial concentration of CEF, the adsorbent dose, and the stirring rate was also investigated using 5% Fe 5% Cu-TiO_2 along with the effect of pH. Apparently, the highest adsorption efficiency (58%) was achieved at 25 and 50 ppm upon testing the effect of the initial concentration of CEF as shown in Fig. 12**.a**. However, the best adsorption was achieved at the highest concentration of 100 ppm as the adsorption capacity was found to be 16.8, 29, 58, 51, and 66 mg/g by increasing the initial concentration from 15 to 100 ppm. At higher concentrations, there is more contact between the CEF solution and the adsorbent surface that facilitates faster transport of CEF molecules towards the adsorbent surface and enhances the adsorption process, which is the opposite of what happens at low concentrations. Additionally, at higher concentrations, CEF molecules have a higher probability of interacting with the active sites on the adsorbent surface, overcoming any potential competitive adsorption from other solutes or interfering species in the wastewater. However, at lower concentrations, the number of CEF molecules is lower, which may allow other competing species or impurities in the wastewater to occupy some of the active sites and reduce the adsorption capacity.

When comparing the obtained adsorption capacity with previously published capacities, many factors should be considered including the solution volume, concentration of pollutants, and the adsorbent dose. Thus, there is a significant variation in the published adsorption capacities of CEF ranging between 844 mg/g [33] to just 0.72 mg/g [34] according to different experimental conditions. So by comparing the obtained capacity in the current study when using 100 ppm of CEF (66 mg/g) with Olusegun et al. [35] who used a similar adsorbent dose (0.01 g) and CEF concentration (100 ppm), but a different volume (15 mL), it was concluded that their adsorption capacity was higher as it was 109 mg/g using ferrihydrite with 10% silica rice husk. Such a significant difference could be attributed to the use of a different material for adsorption. However, the obtained adsorption capacity in this study using 25 ppm of CEF (29 mg/g) was considerably higher than 3.5 mg/g, which is the capacity obtained by Mahmoud et al. [36] who used a titania-based adsorbent (nanotitanium oxide/chitosan/nano-bentonite) and applied the same experimental conditions (Adsorbent dose: 0.01 g, CEF concentration: 25 ppm, volume of solution: 20 mL, and room temperature).

Although the adsorption efficiency increased from 40% to 58% with increasing the dose of 5% Fe 5% Cu-TiO_2 from 0.005 g to 0.01 g as shown in Fig. 12.b, the dose of 0.005 g is considered the most efficient one as the obtained adsorption capacity was 40, 36, and 29 mg/g using 0.005, 0.0075, and 0.01 g, respectively. Investigating the effect of stirring rate showed that by increasing the rate from 0 to 1200 rpm the adsorption efficacy improved from 27% to 59% along with an increase in the adsorption capacity from 13.5 mg/g to 29.5 mg/g (Fig. 12.c). This result could be attributed to the enhanced diffusion rate or mass transfer of CEF molecules towards the adsorbent's surface resulting in an enhanced adsorption of these molecules on the surface of 5% Fe 5% Cu-TiO_2.

3.4.4. Application of 5% Fe 5% Cu-TiO_2 in the adsorption of CEF from tap and real wastewater samples

A step towards investigating the applicability of the abovementioned TiO_2 composite (5% Fe 5% Cu-TiO_2) in different water samples was

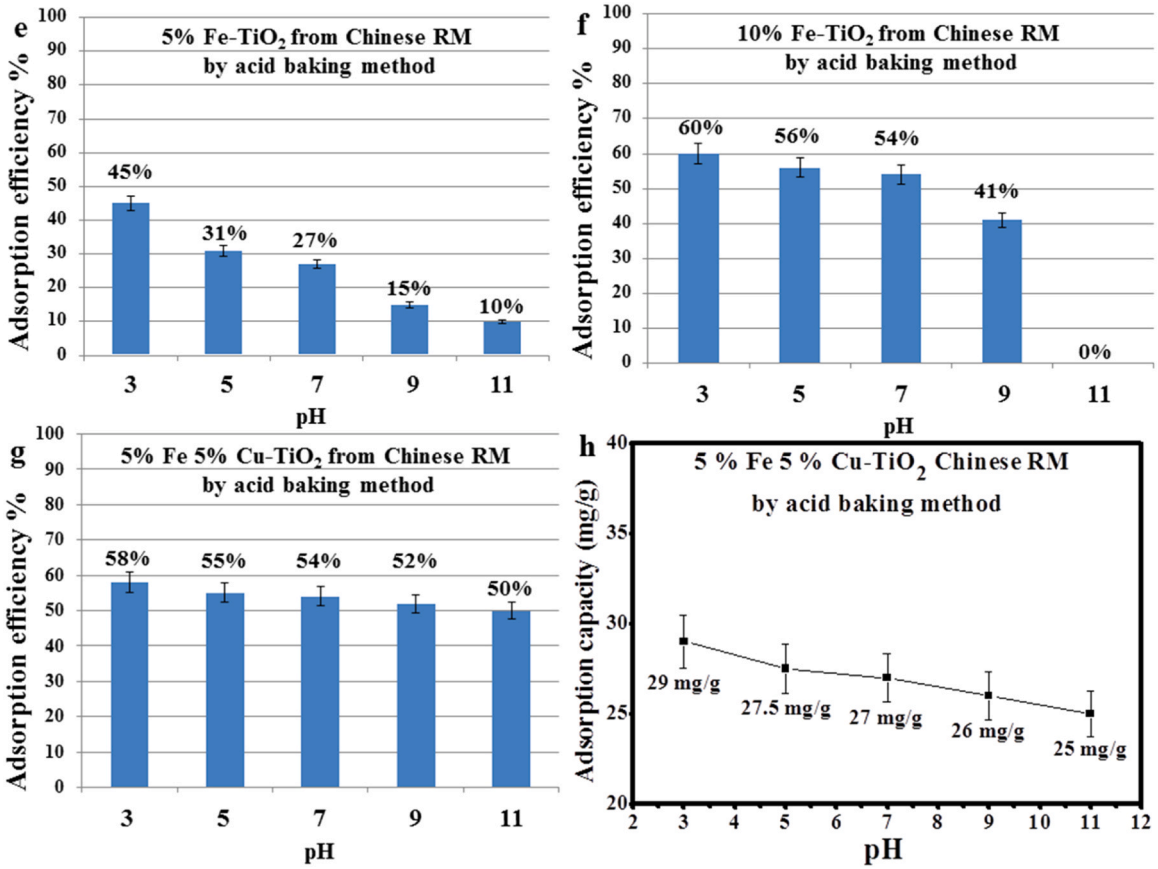

Fig. 7. (*continued*).

undertaken by testing the adsorption efficiency of this composite in removing CEF from tap water samples. Although the adsorption efficiency of 5% Fe 5% Cu-TiO_2 in tap water at pH 3 was the highest with an efficiency of 51% and an adsorption capacity of 25.5 mg/g similar to that observed using deionized water, the adsorption trend was different as the efficiency decreased at pH 5, followed by a slight increase at pH 7 and 9, and then it remained constant at pH 11 as shown in Fig. 12.d. Such an irregular adsorption trend could be attributed to the presence of other organic and inorganic pollutants in water matrix. So all in all, the applicability of 5% Fe 5% Cu-TiO_2 in adsorbing CEF from tap water samples over the whole pH range was verified based on the observed results. Furthermore, the applicability of this adsorbent in treating real wastewater samples has not been investigated yet as it is not that easy to get these samples in the meantime. However, this point is suggested to be further investigated in future work as there could be a different adsorption trend compared to those observed when using deionized water and tap water.

3.4.5. *ICP analysis*

The concentration of leached iron and copper metals from 5% Fe 5% Cu-TiO_2 was measured by ICP analysis to determine the effect of using them in wastewater treatment. As shown in Fig. 13.a, there is no actual trend in the concentration of leached iron as it was decreasing and increasing by increasing the pH from 3 up to 11. Although the water resulting from the currently used adsorption process will not be directly used for drinking, it is important to note that the concentration of leached iron was within the limits of the World Health Organization (WHO) for iron ions in drinking water that is 0.3 ppm over most of the pH levels except for pH 7 and 11. In Fig. 13.b, the concentration of leached copper from the same composite was decreasing by increasing the pH from 3 to 9, but it slightly increased at pH 11. Also, it has to be mentioned that the concentration of leached copper was close to the WHO limit of copper ions in drinking water that is 2 ppm except for pH 3. Therefore, it was concluded that 5% Fe 5% Cu-TiO_2 could be safely used in adsorbing CEF molecules from wastewater in different acidic, neutral, and alkaline conditions, and more precisely at pH 5 and 9. It has to be mentioned that synthesizing single-atom catalysts using tiny amounts of metals' loading is a recent strategy used to solve the issue of metals' leaching during wastewater treatment. Therefore, it is planned to investigate the applicability of the currently synthesized Cu and Fe-TiO_2 composites as single-atom catalysts and the Fe-Cu-TiO_2 composite as a double-atom catalyst in the degradation of CEF molecules in future studies. Such a plan is based on the acceptable adsorption efficiencies of the composites, so the possible synergistic effect of adsorption, which is usually undertaken prior to any type of catalytic degradation, combined with the catalytic degradation could result in very high removal efficiencies. Also, it should be mentioned that no regeneration studies were conducted in this work and this point would be addressed after investigating the enhancement of removal efficiencies by synthesizing the single and double-atom based materials.

3.4.6. *Adsorption mechanism of CEF by TiO_2 composites*

Generally, there are different mechanisms in any adsorption process that contribute to the removal of pollutants such as electrostatic attraction. The CEF species at pH 3 and higher was used in Fig. 14 as it was the most adsorbed species in the current study. As it was indicated in the speciation of CEF molecules in Section 3.4.1 that CEF molecules start to be negatively charged at pH higher than 2. Therefore, the electrostatic attraction at pHs higher than 2 between the positively charged TiO_2 that has a PZC of 4 and the negatively charged CEF molecules could be responsible for the adsorption of CEF molecules. This electrostatic attraction was further enhanced by impregnating TiO_2 with 10% Cu, 10% Fe, and 5% Fe 5% Cu as indicated by the higher PZC values of 10% Cu-TiO_2, 10% Fe-TiO_2, and 5% Fe 5% Cu-TiO_2 that were 6.3, 4.2, and

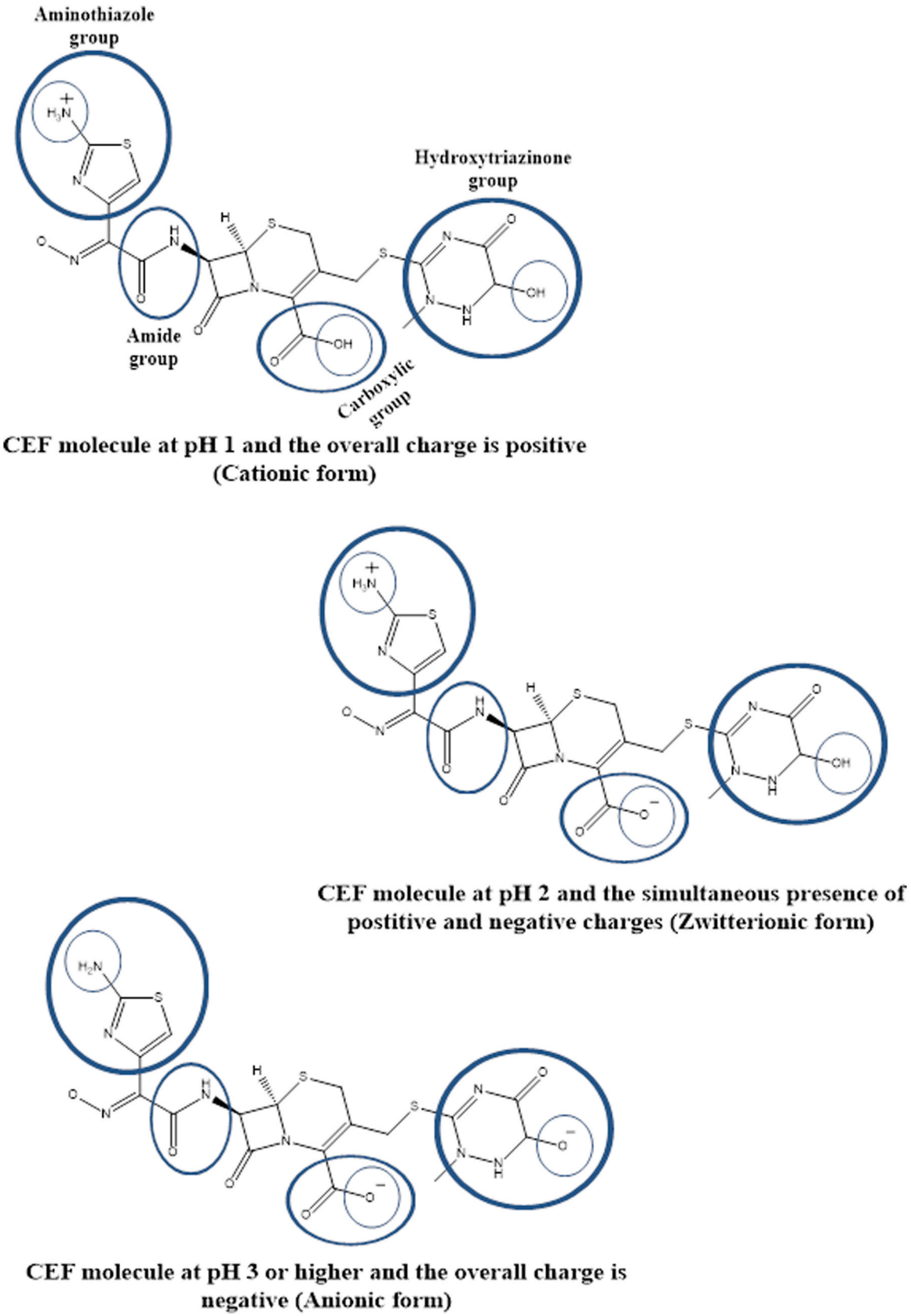

Fig. 8. A proposed speciation of CEF molecules at different pH levels and their overall surface charge.

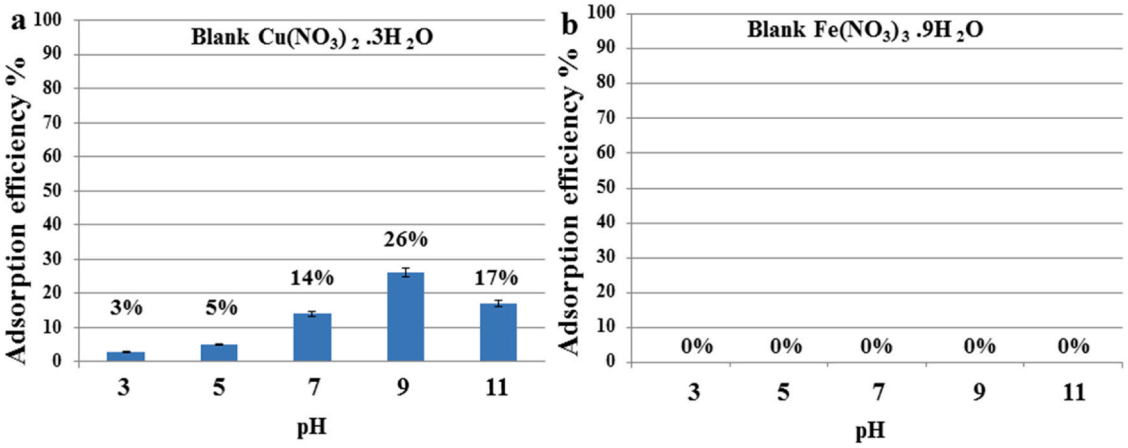

Fig. 9. Blank experiments of CEF adsorption efficiency by $Cu(NO_3)_2.3\ H_2O$ **(a)** and $Fe(NO_3)_3.9\ H_2O$ **(b)** after 30 min. [C_o = 25 ppm, stirring rate = 800 rpm, T = 25 °C, and dose = 0.01 g].

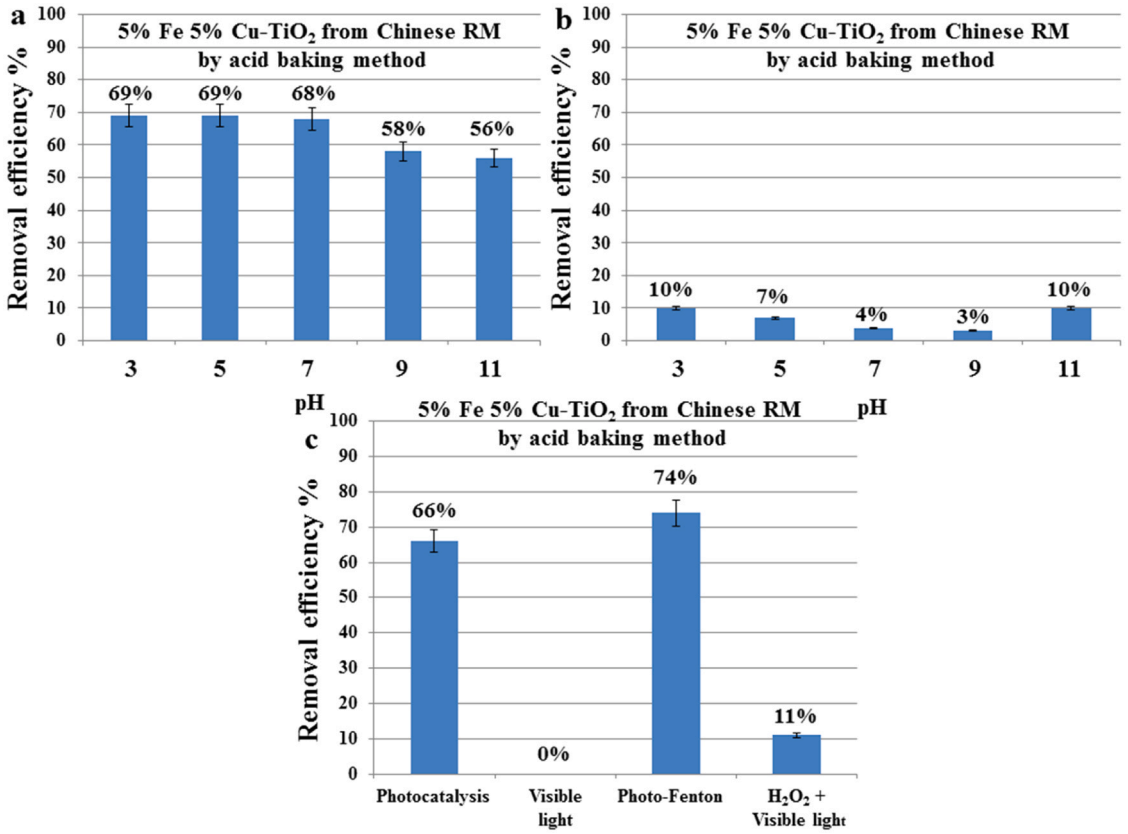

Fig. 10. The catalytic degradation efficiency of CEF molecules by 5% Fe 5% Cu-TiO_2 using H_2O_2 over the whole pH range (a), blank experiments of CEF degradation efficiency by H_2O_2 over the whole pH range (b), the photocatalytic degradation efficiency of CEF molecules using 5% Fe 5% Cu-TiO_2 at pH 3, a blank experiment using visible light at pH 3, the photo-Fenton catalytic degradation efficiency of CEF molecules using 5% Fe 5% Cu-TiO_2 at pH 3, and a blank experiment using H_2O_2 and visible light at pH 3 (c). [C_o = 25 ppm, stirring rate = 800 rpm, T = 25 °C, and dose = 0.01 g].

5.8, respectively, resulting in improving the adsorption efficiency. However, the efficiency decreased by increasing the pH level beyond the abovementioned PZC values due to the electrostatic repulsion between the negatively charged adsorbents and CEF molecules as already discussed in Section 3.4.1.

Another mechanism that may be contributing to the adsorption process is coordination, which is achieved by the donation of pairs of electrons from the functional groups of CEF molecules such as the oxygen atom of the carboxylate group or the nitrogen atom of the amino group. The strength of the coordinate bond can vary depending on the specific ligands and coordination environment. In general, Cu^{2+} and Fe^{3+} can have a coordination number of up to 6 with CEF molecules [37]. Furthermore, the higher positive charge of Fe^{3+} compared to Cu^{2+} could result in more electrostatic attraction to negatively charged species.

FTIR analysis was used to further investigate the coordination between CEF molecules and 5% Fe 5% Cu-TiO_2 experimentally. As shown in Fig S1**.a** a broad band of an O-H group appeared in the spectrum of CEF solution at 3300 cm^{-1} before the adsorption process, which remained as it is after the adsorption process (Fig S1**.b**) since it mainly

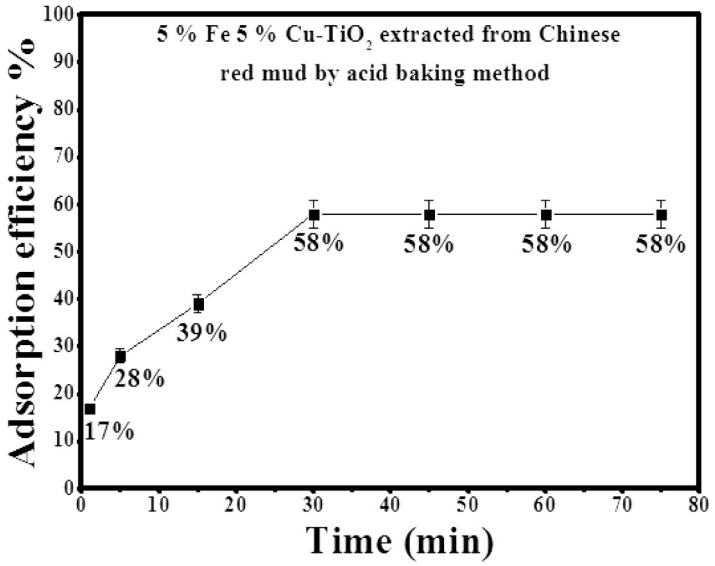

Fig. 11. Effect of time in CEF adsorption by 5% Fe 5% Cu-TiO_2. [C_o = 25 ppm, pH = 3, stirring rate = 800 rpm, T = 25 °C, and dose = 0.01 g].

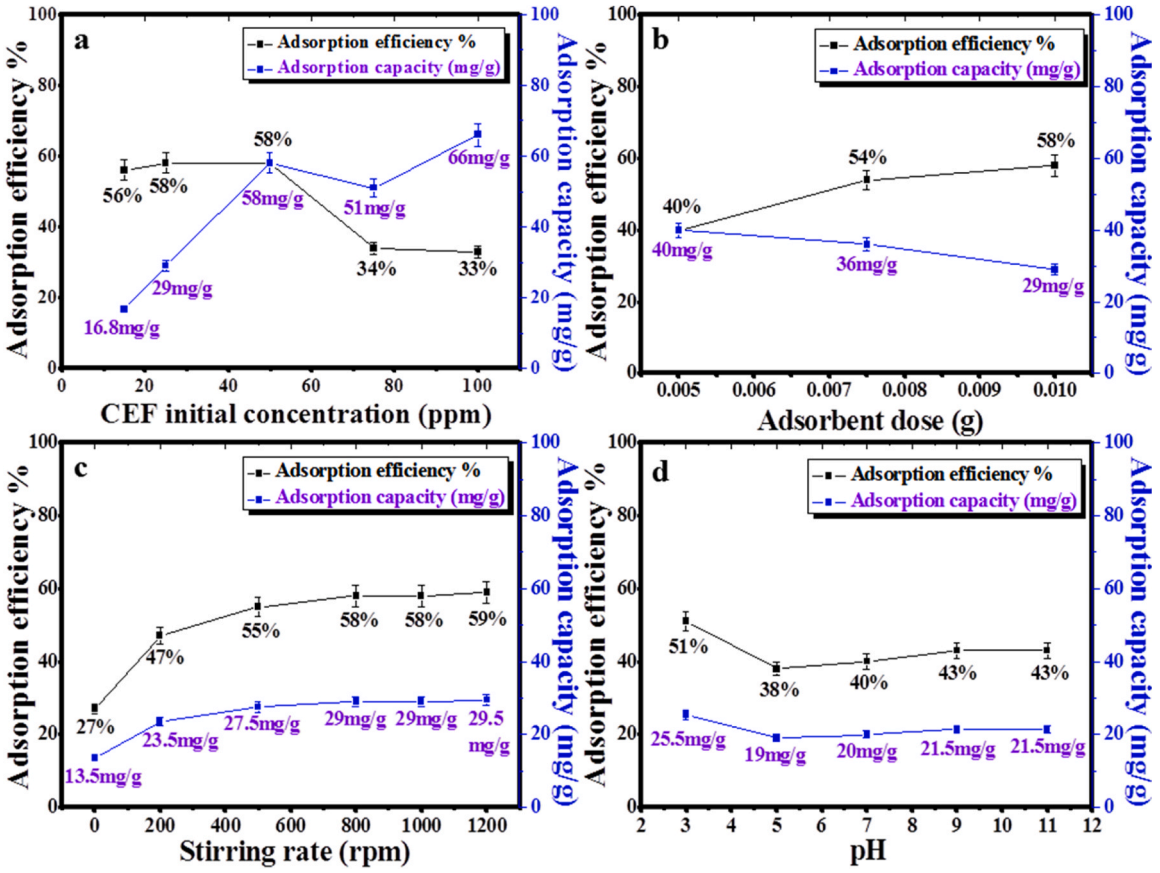

Fig. 12. Effect of variation in initial concentration of CEF after 30 min using 5% 5% Cu-TiO_2 (a) [pH = 3, stirring rate = 800 rpm, T = 25 °C, and dose = 0.01 g], 5% 5% Cu-TiO_2 dose (b) [C_o = 25 ppm, pH = 3, stirring rate = 800 rpm, and T = 25 °C], stirring rate of 5% 5% Cu-TiO_2 on the adsorption efficiency and capacity of CEF (c) [C_o = 25 ppm, pH = 3, T = 25 °C, and dose = 0.01 g], and CEF adsorption efficiency and capacity by 5% Fe 5% Cu-TiO_2 in tap water sample (d) [C_o = 25 ppm, stirring rate = 800 rpm, T = 25 °C, and dose = 0.01 g].

results from water that is used as a solvent to dissolve the solid powder of CEF. The carbonyl group (C═O) feature of CEF can be observed before the adsorption process at 1650 cm^{-1} (Fig S1.**a**) whose intensity slightly decreased after the adsorption (Fig S1.**b**) indicating the possible coordination between the oxygen atoms of CEF and the adsorbent. The spectrum of 5% Fe 5% Cu-TiO_2 showed a Ti-O peak at ca. 1075 cm^{-1} as shown in Fig S1.**c**, whose intensity decreased after the adsorption process as can be seen in Fig S1.**d**. The appearance of a Ti-O band after the adsorption process (Fig S1.**b**) possibly indicated the coordination between Ti species in 5% Fe 5% Cu-TiO_2 and the oxygen species in CEF.

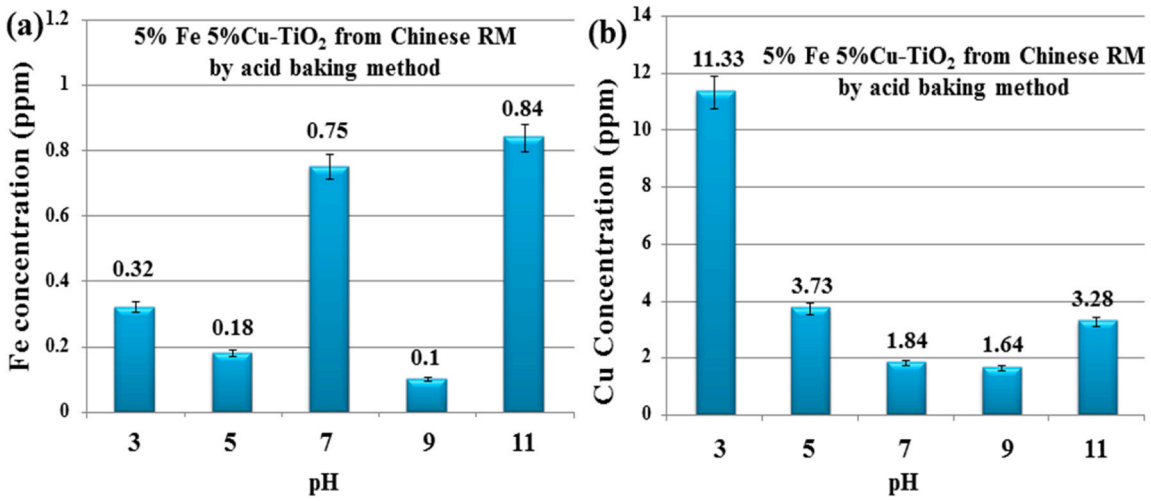

Fig. 13. The concentration of leached iron (a) and leached copper (b) from 5% Fe 5% Cu-TiO_2 as determined by ICP analysis. [C_o = 25 ppm, stirring rate = 800 rpm, T = 25 °C, dose = 0.01 g, and time = 30 min].

One further mechanism is the synergistic effect between the residues of metal salt precursors and TiO_2 that is reckoned as one of the forces that enhanced the adsorption efficiency of CEF in the current study. This effect was confirmed by running blank experiments using copper and iron nitrates as previously discussed in Section 3.4.1. The results confirmed the adsorption of CEF using copper nitrate as shown in Fig. 9. However, iron nitrate did not show any removal efficiency, explaining why Fe-TiO_2 complexes had low efficiency at alkaline pH levels, whereas 5% Fe 5% Cu-TiO_2 showed the synergistic effect of both metals over the whole pH range. Further studies are required to further clarify the adsorption mechanism, which will be undertaken in future work.

3.5. *The economic analysis of producing TiO_2 and 5% Fe 5% Cu-TiO_2*

Producing TiO_2 and 5% Fe 5% Cu-TiO_2 was a simple procedure developed on a laboratory scale, eliminating the need for high levels of technology or extensive labor. Thus, expenses associated with labor wages, taxes, maintenance, and management were not considered in this very rough calculation. The main factors in calculating the production cost of one g of any material include the prices of the used chemicals, water, and electricity charges.

Regarding the chemical cost required to produce one g of TiO_2 by the alkali roasting method would be approximately 1.01 pounds and the calculation is as follow: 2.50 liters of H_2SO_4 currently costs 40.30 sterling pounds [38], so the used 10 mL in the current study are 0.16 pounds. 500 g of CaO currently costs 66.20 pounds [39], so the 5 g used in this study are 0.66 pounds. 500 g of Na_2CO_3 currently costs 19.10 pounds [40], so the used 5 g are 0.19 pounds. The chemicals' prices are available on the suppliers official websites. In addition, an average of 10 L of water was estimated to be used for washing, neutralizing, and extracting TiO_2 would cost 0.06 pounds. The water cost is based on the charges provided [41] including both water and wastewater charges in the fiscal year of 2023/2024. Furthermore, the current standard charge of electricity per day is 0.62 pounds [42], which is assumed to be the average cost of the total number of hours of using the electric furnaces and ovens in this work. Therefore, the total cost of producing one g of TiO_2 by alkali roasting method would be around 1.69 pounds.

For the production cost of one g of TiO_2 by the acid baking method, it would be the same as the alkali roasting method, but without CaO and Na_2CO_3, so the total cost of this method is about 0.84 pounds. The cost of chemicals used in modifying one g of TiO_2 extracted using acid baking method by 5%Fe5%Cu would be just 0.06 pounds. In detail, 500 g of Fe$(NO_3)_3(H_2O)_9$ currently costs 46.60 pounds [43], so 5% of iron contained in 0.36 g of this salt based on using 1 g of TiO_2 is 0.03 pounds. 500 g of Cu$(NO_3)_2(H_2O)_3$ from currently costs 90.37 pounds [44], so 5% of this salt (0.19 g) based on using 1 g of TiO_2 is 0.03 pounds. Thus, the total cost of producing one g of 5% Fe 5% Cu-TiO_2 would be around 0.90 pounds.

The cost of 50 g of commercial TiO_2 (P 25) is currently 78.6 pounds [45], so 1 g costs about 1.57 pounds. Therefore, by comparing the costs of commercial TiO_2 by that extracted using the acid baking method and its composite (5% Fe 5% Cu-TiO_2), it is apparent that these two materials are cheaper and with higher adsorption efficiency confirming their economic potential.

4. Conclusions

In the recent investigations into the viability of using TiO_2 extracted from Chinese red mud for adsorption purposes, a promising performance has been observed in the current study, exhibiting a generally better efficiency compared to its commercial counterpart, P25. XRD analysis revealed a purer crystalline phase composition of TiO_2 extracted by the acid baking method compared to the alkali roasting method, which resulted in a better adsorption efficiency. Different percentages of iron and copper ions were used in impregnating TiO_2 to improve its adsorption efficiency and among them, 5% Fe 5% Cu-TiO_2 was shown to be the best adsorbent as it resulted in adsorbing more than 50% of CEF molecules over most of the pH range. The adsorption mechanism was suggested to be based on electrostatic attractions, van der Waals forces, complexation processes, and a synergistic effect between TiO_2 and metal salt precursors. Regarding the safety parameter of applying heavy metals in adsorbing CEF molecules, ICP analysis revealed that the leaching of iron and copper ions from 5% Fe 5% Cu-TiO_2 is in alignment with the WHO standards under various conditions; specifically at pH 5 and 9. Synthesizing single and double-atom catalysts using the materials reported in this work is planned in future work to make use of their acceptable adsorption efficiencies and solving the metals' leaching issue. This plan is also based on the catalytic and photocatalytic degradation efficiencies of 5% Fe 5% Cu-TiO_2 in the current study, which were not that promising. Moreover, a simple very crude economic analysis confirmed the economic efficiency of TiO_2 and 5% Fe 5% Cu-TiO_2 produced by the acid baking method compared to the commercial TiO_2. Therefore, the current results pave the way for a sustainable solution in turning a highly alkaline waste material such as red mud into an adsorbent that can be efficiently used in wastewater treatment.

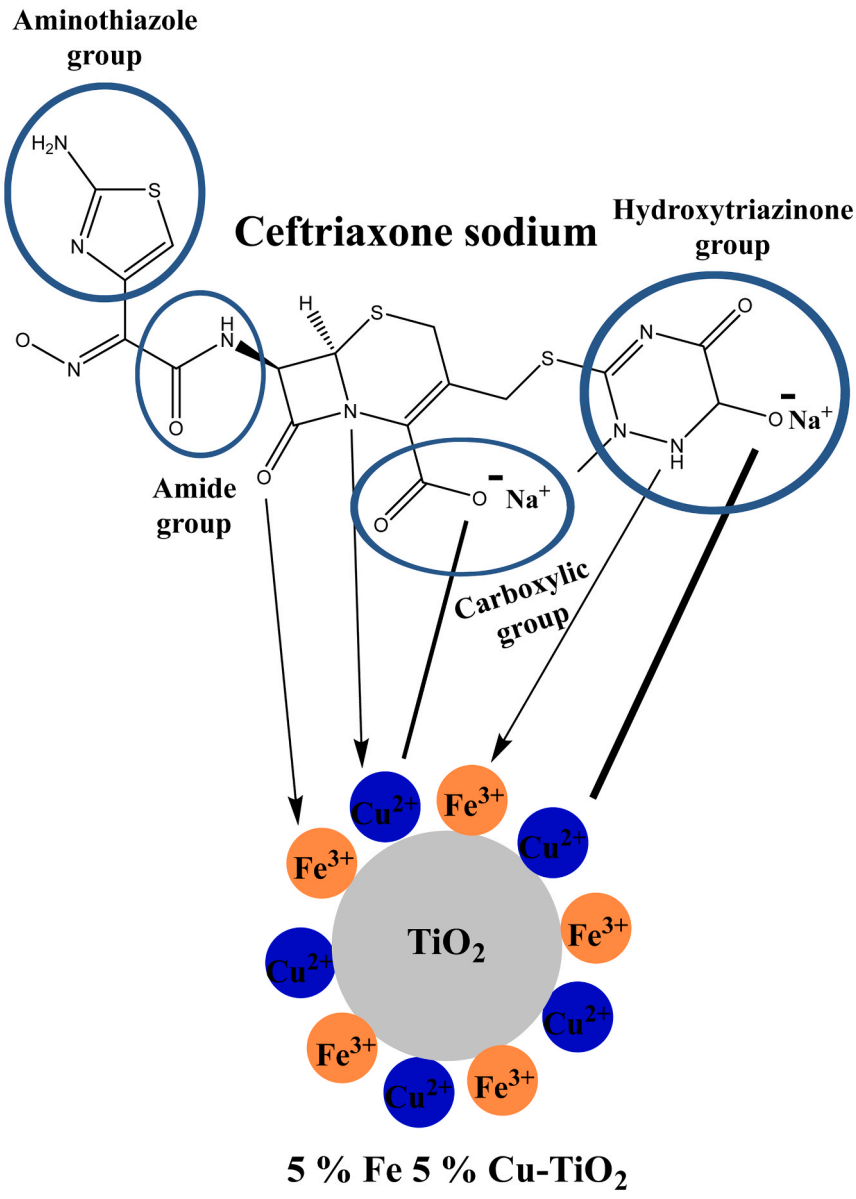

Fig. 14. A proposed adsorption mechanism of CEF using 5% Fe 5% Cu-TiO_2.

CRediT authorship contribution statement

Hosny Mohamed: Writing – original draft, Visualization, Investigation, Formal analysis, Data curation, Conceptualization. **Hargreaves Justin S J:** Writing – review & editing, Validation, Supervision, Investigation, Conceptualization.

Declaration of Competing Interest

The authors declare that they have no known competing financial interests or personal relationships that could have appeared to influence the work reported in this paper.

Data availability

Data will be made available on request.

Acknowledgments

The researcher (Mohamed Hosny) is funded by a full scholarship (MM32/21) from the Egyptian Ministry of Higher Education & Scientific Research represented by the Egyptian Bureau for Cultural & Educational Affairs in London. The authors would like to thank Dr Hannian Gu for his very kind help in providing the red mud sample used in this study.

Appendix A. Supporting information

Supplementary data associated with this article can be found in the online version at doi:10.1016/j.cattod.2024.114539.

References

[1] L. Liang, Z. Wang, J. Li, The effect of urbanization on environmental pollution in rapidly developing urban agglomerations, J. Clean. Prod. 237 (2019) 117649.
[2] E.M. Abd El-Monaem, et al., A comprehensive review on LDH-based catalysts to activate persulfates for the degradation of organic pollutants, npj Clean. Water 6 (1) (2023) 34.
[3] M. Wang, X. Liu, Applications of red mud as an environmental remediation material: a review, J. Hazard. Mater. 408 (2021) 124420.
[4] Statista, 2021. Production of alumina worldwide in 2021, by country (in 1,000 metric tons). https://www.statista.com/statistics/264963/global-alumina-production-by-country/ (Accessed 12 October 2022). 2021.

[5] E. Mukiza, et al., Utilization of red mud in road base and subgrade materials: a review, Resour. Conserv. Recycl. 141 (2019) 187–199.
[6] M.A. Khairul, J. Zanganeh, B. Moghtaderi, The composition, recycling and utilisation of Bayer red mud, Resour. Conserv. Recycl. 141 (2019) 483–498.
[7] Y. Liu, C. Lin, Y. Wu, Characterization of red mud derived from a combined Bayer Process and bauxite calcination method, J. Hazard. Mater. 146 (1-2) (2007) 255–261.
[8] A. Gelencsér, et al., The red mud accident in Ajka (Hungary): characterization and potential health effects of fugitive dust, Environ. Sci. Technol. 45 (4) (2011) 1608–1615.
[9] Y. Ma, C. Si, C. Lin, Capping hazardous red mud using acidic soil with an embedded layer of zeolite for plant growth, Environ. Technol. 35 (18) (2014) 2314–2321.
[10] S. Wang, et al., Comprehensive utilization status of red mud in China: a critical review, J. Clean. Prod. 289 (2021) 125136.
[11] S. Rai, et al., Disposal practices and utilization of red mud (Bauxite Residue): a review in Indian context and abroad, J. Sustain. Metall. 6 (1) (2020) 1–8.
[12] A. Russkikh, et al., Turning waste into value: potassium-promoted red mud as an effective catalyst for the hydrogenation of Co2, ChemSusChem 13 (11) (2020) 2981–2987.
[13] M.A. Camilleri, A circular economy strategy for sustainable value chains: a European perspective, in: S. Vertigans, S.O. Idowu (Eds.), Global Challenges to CSR and Sustainable Development: Root Causes and Evidence from Case Studies, Springer International Publishing, Cham, 2021, pp. 141–161.
[14] M. Pelaez, et al., A review on the visible light active titanium dioxide photocatalysts for environmental applications, Appl. Catal. B Environ. 125 (2012) 331–349.
[15] Y. Gan, et al., Impact of Cu particles on adsorption and photocatalytic capability of mesoporous Cu@TiO2 hybrid towards ciprofloxacin antibiotic removal, J. Taiwan Inst. Chem. Eng. 96 (2019) 229–242.
[16] S. Sanguanpak, et al., TiO2-immobilized porous geopolymer composite membrane for removal of antibiotics in hospital wastewater, Chemosphere 307 (2022) 135760.
[17] D. O'Flynn, et al., A review of pharmaceutical occurrence and pathways in the aquatic environment in the context of a changing climate and the COVID-19 pandemic, Anal. Methods 13 (5) (2021) 575–594.
[18] E.M. Abd El-Monaem, et al., Sustainable adsorptive removal of antibiotic residues by chitosan composites: an insight into current developments and future recommendations, Arab. J. Chem. 15 (5) (2022) 103743.
[19] M. Hosny, M. Fawzy, Sustainable synthesis of a novel hydrothermally carbonized AuNPs-hydrochar nanocomposite for the photocatalytic degradation of cephalexin, Biomass-.-. Convers. Biorefinery (2023) 1–18.
[20] E.M. Abd El-Monaem, M. Hosny, A.S. Eltaweil, Synergistic effect between adsorption and Fenton-like degradation on CoNiFe-LDH/ZIF-8 composite for efficient degradation of doxycycline, Chem. Eng. Sci. 287 (2024) 119707.
[21] M. Hosny, M. Fawzy, A.S. Eltaweil, Phytofabrication of bimetallic silver-copper/biochar nanocomposite for environmental and medical applications, J. Environ. Manag. 316 (2022) 115238.
[22] J. Yang, X. Luo, Ag-doped TiO2 immobilized cellulose-derived carbon beads: one-pot preparation, photocatalytic degradation performance and mechanism of ceftriaxone sodium, Appl. Surf. Sci. 542 (2021) 148724.
[23] G. Li, et al., Stepwise extraction of valuable components from red mud based on reductive roasting with sodium salts, J. Hazard. Mater. 280 (2014) 774–780.
[24] S. Agrawal, N. Dhawan, Microwave acid baking of red mud for extraction of titanium and scandium values, Hydrometallurgy 204 (2021) 105704.
[25] T. Mahmood, et al., Comparison of different methods for the point of zero charge determination of NiO, Ind. Eng. Chem. Res. 50 (17) (2011) 10017–10023.
[26] S. Abbasi, Photocatalytic activity study of coated anatase-rutile titania nanoparticles with nanocrystalline tin dioxide based on the statistical analysis, Environ. Monit. Assess. 191 (4) (2019) 206.
[27] H. Gu, N. Wang, J.S.J. Hargreaves, Sequential extraction of valuable trace elements from bayer process-derived waste red mud samples, J. Sustain. Metall. 4 (1) (2018) 147–154.
[28] E.K. Güner, A.K. Özer, Synthesis and characterization of copper hydroxynitrate by hydrothermal method, J. Turk. Chem. Soc. Sect. B Chem. Eng. 1 (1) (2017) 183–192.
[29] A. Di Paola, et al., Preparation of polycrystalline TiO2 photocatalysts impregnated with various transition metal ions: characterization and photocatalytic activity for the degradation of 4-nitrophenol, J. Phys. Chem. B 106 (3) (2002) 637–645.
[30] H. Abdelouahab Reddam, et al., Synthesis of Fe, Mn and Cu modified TiO2 photocatalysts for photodegradation of Orange II, Bol. De. la Soc. Esp. De. Cerámica Y. Vidr. 59 (4) (2020) 138–148.
[31] M. Aleksić, et al., Acidity constants of cefetamet, cefotaxime and ceftriaxone; the effect of the substituent at C3 position, J. Pharm. Biomed. Anal. 39 (3) (2005) 752–756.
[32] N.M. Zaki, M.M. Hafez, Enhanced antibacterial effect of ceftriaxone sodium-loaded chitosan nanoparticles against intracellular Salmonella typhimurium, Aaps Pharmscitech 13 (2012) 411–421.
[33] M. Abdullah, et al., Removal of ceftriaxone sodium antibiotic from pharmaceutical wastewater using an activated carbon based TiO2 composite: adsorption and photocatalytic degradation evaluation, Chemosphere 317 (2023) 137834.
[34] M. Dávila-Estrada, et al., Kinetic and equilibrium sorption studies of ceftriaxone and paracetamol by surfactant-modified zeolite, Water Air Soil Pollut. 229 (2018) 1–9.
[35] S.J. Olusegun, N.D. Mohallem, V.S. Ciminelli, Reducing the negative impact of ceftriaxone and doxycycline in aqueous solutions using ferrihydrite/plant-based composites: mechanism pathway, Environ. Sci. Pollut. Res. 29 (44) (2022) 66547–66561.
[36] M.E. Mahmoud, et al., Enhanced adsorption of Levofloxacin and Ceftriaxone antibiotics from water by assembled composite of nanotitanium oxide/chitosan/nano-bentonite, Mater. Sci. Eng.: C. 108 (2020) 110199.
[37] M.S. Refat, et al., In neutralized medium five new Ca(II), Zn(II), Fe(III), Au(III) and Pd(II) complexity of ceftriaxone antibiotic drug: Synthesis, spectroscopic, morphological and anticancer studies, J. Mol. Liq. 322 (2021) 114816.
[38] Sulfuric Acid, 96% Solution in Water, Extra Pure, Thermo Scientific Chemicals. 2024 [cited 2024 05 January 2024]; Available from: https://www.fishersci.co.uk/shop/products/sulfuric-acid-96-solution-water-extra-pure-thermo-scientific/10715801#?keyword=.
[39] Calcium oxide, Reagent Grade, Thermo Scientific Chemicals, 2024 [cited 2024 05 January 2024]; Available from: https://www.fishersci.co.uk/shop/products/calcium-oxide-reagent-grade-thermo-scientific/11317618#?keyword=calcium%20oxide.
[40] Sodium carbonate, 98%, Thermo Scientific Chemicals. 2024 [cited 2024 05 January 2024]; Available from: https://www.fishersci.co.uk/shop/products/sodium-carbonate-98-thermo-scientific/11317886#?keyword=sodium%20carbonate.
[41] Metered Household Charges 2023/24, 2023 [cited 2024 05 January 2024]; Available from: https://www.scottishwater.co.uk/Help-and-Resources/Document-Hub/Your-Home/Charges.
[42] Tarrif information labels, 2023 [cited 2024 05 January 2024]; Available from: https://www.scottishpower.co.uk/tariff-information-labels/tariff-information-label/5788.
[43] Iron(III) nitrate nonahydrate, ACS, 98.0–101.0%, Thermo Scientific Chemicals. 2024 [cited 2024 05 January 2024]; Available from: https://www.thermofisher.com/order/catalog/product/033315.36?SID=srch-srp-033315.36.
[44] Copper(II) nitrate trihydrate, 2024 [cited 2024 05 January 2024]; Available from: https://lab.honeywell.com/shop/copper-ii-nitrate-trihydrate-61194.
[45] Titanium(IV) oxide, Aeroxide(R) P25, Thermo Scientific Chemicals. 2024 [cited 2024 05 January 2024]; Available from: https://www.thermofisher.com/order/catalog/product/384290500?SID=srch-srp-384290500.